

# Variability of black hole accretion discs: The cool, thermal disc component

M. Mayer<sup>1</sup> & J. E. Pringle

*Institute of Astronomy, Madingley Road, Cambridge CB30HA, UK*

<sup>1</sup> *E-Mail: mm@ast.cam.ac.uk*

31 October 2018

## ABSTRACT

We extend the model of King et al. (2004) for variability in black hole accretion discs, by taking proper account of the thermal properties of the disc. Because the degree of variability in the King et al. (2004) model depends sensitively on the ratio of disc thickness to radius,  $H/R$ , it is important to follow the time-dependence of the local disc structure as the variability proceeds. In common with previous authors, we develop a one-zone model for the local disc structure. We agree that radial heat advection plays an important role in determining the inner disc structure, and also find limit-cycle behaviour. When the stochastic magnetic dynamo model of King et al. (2004) is added to these models, we find similar variability behaviour to before.

We are now better placed to put physical constraints on model parameters. In particular, we find that in order to be consistent with the low degree of variability seen in the thermal disc component of black hole binaries, we need to limit the energy density of the poloidal field that can be produced by local dynamo cells in the disc to less than a few percent of the energy density of the dynamo field within the disc itself.

**Key words:** black hole physics – galaxies: jets – X-Rays: binaries.

## 1 INTRODUCTION

Accretion powered x-ray sources, both on the galactic (AGN) and stellar (X-ray binaries) scales, display significant aperiodic variability, or flickering, on a broad range of timescales (see for example McHardy 1988; Belloni & Hasinger 1990; van der Klis 1994; Markowitz et al. 2003; Vaughan et al. 2003; McClintock & Remillard 2004). The origin of this variability is not well understood. However, Uttley (2004) and Uttley et al. (2005) have pointed out that the existence of a strong linear relationship between the amplitude of the X-ray variability and the amplitude of the x-ray flux (Uttley & McHardy 2001) – the rms-flux relation – can be used as a diagnostic to distinguish between various models. For example Uttley et al. (2005) emphasise that the standard simple shot-noise models, where the light curve is produced by the summation of randomly occurring shots, or flares, cannot explain such a relation. Both Uttley (2004) and Uttley et al. (2005) note that such a relation can be produced naturally by the model of Lyubarskii (1997) where the variability is produced by variations in the accretion rate occurring at different radii which propagate inwards, and so modulate the energy release in the central x-ray emitting region. The major problem with this model, as noted by Lyubarskii (1997), is the physical origin of the accretion rate variations. In order for the model to work, as also emphasised by Churazov et al. (2001), it is necessary for the timescale of the variations at each radius to be at least as long as the viscous timescale at that radius. The most obvious origin for fluctuations in an accretion disc are turbulent

or hydro-magnetic, perhaps associated with the disc dynamo, and these take place on the local dynamical timescale ( $\sim \Omega^{-1}$ , where  $\Omega$  is the angular velocity), which is shorter than the local viscous timescale by a factor of  $\sim \alpha(H/R)^2$ , where  $\alpha$  ( $<1$ ) is the viscosity parameter, and  $H/R < 1$  the disc opening angle (Pringle 1981).

A solution to this problem, in the form of an explicit physical model, has been recently proposed by King et al. (2004), based on ideas put forward by Livio et al. (2003). They suggest that the local dynamo processes in the disc can affect the accretion rate by driving angular momentum loss in the form of an outflow (wind or jet). They model the dynamo as a small-scale stochastic phenomenon, operating on roughly the local dynamical timescale. They then postulate that large-scale outflow can only occur when small-scale random processes in neighbouring disc annuli give rise by chance to a coherent large-scale field. This occurs on much longer timescales, by a factor of order  $2^{R/H}$  (Livio et al. 2003). This also provides an explanation for why the dominant flickering frequencies are typically much longer than the dynamical timescales at the centre of the disc where most of the energy is released.

However, King et al. (2004) took a very idealised model for the disc in that they assumed that the disc had a constant thickness ratio of  $H/R$ . This simplified the computations for two main reasons. First, local disc structure equations could be ignored, because there was no need to compute the local value of disc thickness. Second, because the local disc dynamos were assumed to be spatially independent on a radial scale of  $\Delta R \sim H$ , there was

no need to vary the number of independent dynamos as the disc thickness varied with time. In this paper we take the first steps towards remedying this deficiency. For the time being we concern ourselves with a standard (optically thick, geometrically thin) accretion disc, and thus any conclusions we have will be relevant mainly to the thermally dominated (TD) state of the X-ray transients (e.g. McClintock & Remillard 2004). We leave the extension to the more interesting, and more variable (low/hard) state, containing both disc and corona, to future work. In Section 2 we explain how we generalise the work of King et al. (2004) by including equations to compute the local disc structure, and also explain how we vary the grid spacings to follow the radial size of the local disc dynamo cells in such a way as to minimise unwanted numerical mixing. In Sections 3 and 4 we investigate the models which result from our equations when there is a steady external accretion rate, and in Section 5 compare our results with previous work in the field. In Section 6 we add the variability according to the stochastic magnetic model of King et al. (2004). In Section 7, we discuss the observational data on the variability of the thermal disc component, to which our models are relevant, and in Section 8 we show that for expected values of the model parameters our models are consistent with the data. We present brief conclusions in Section 9.

## 2 METHODOLOGY

In this Section we present the input physics for our basic accretion disc models. For a more detailed discussion, see for example Frank et al. (2002).

The disc is treated as one-dimensional, in the sense that we resolve the disc in radial direction only, dividing the disc into annuli, and just use the one-zone approximation in the vertical direction. Thus, all variables (e.g. mass density  $\rho$ , temperature  $T$  etc.) have one value at each radius  $R$ , and we make no further assumptions about the vertical disc structure. Thus, for example the surface density  $\Sigma$  is given in terms of density  $\rho$  and disc semi-thickness  $H$  by the relation

$$\Sigma = 2\rho H \quad (1)$$

As we discuss in Section 5 it is possible to make more detailed assumptions about the vertical disc structure. However, in view of the large number of uncertainties in the basic physical processes involved here, we regard such extra complications as unnecessary for our current purposes.

### 2.1 Surface density

The viscous evolution of the disc is governed (Pringle 1981; Livio & Pringle 1992) by the equation of continuity

$$\frac{\partial \Sigma}{\partial t} + \frac{1}{R} \frac{\partial}{\partial R} (\Sigma R u_R) = 0 \quad (2)$$

and by the equation of conservation of angular momentum

$$\frac{\partial}{\partial t} (\Sigma R^2 \Omega_K) + \frac{1}{R} \frac{\partial}{\partial R} (\Sigma R u_R R^2 \Omega_K) = \frac{1}{2\pi R} \frac{\partial G}{\partial R}. \quad (3)$$

Here  $\Sigma$  is the surface density,  $u_R$  the radial velocity,  $\dot{M} = 2\pi \Sigma R u_R$  the accretion rate,  $\Omega_K = \sqrt{GM/R^3}$  the Keplerian rotation frequency and  $G$  the viscous torque.

We should note two things here. First, although we are discussing accretion discs around black holes in this paper, we use

purely Newtonian gravity, around a point mass  $M$ , and truncate the disc at an appropriate radius  $R_{\text{in}} = 6GM/c^2$ . Here again we take the view that the wealth of uncertainties inherent in the physical processes involved, and the complicated nature of the subsequent behaviour, means that adding the complication of using the proper space-time geometry is not warranted at this stage. Second, by taking the angular velocity of the disc material to be  $\Omega_K = \sqrt{GM/R^3}$  we have also neglected the effects of any radial pressure gradient in the disc. We shall show below that this approximation is justified for the disc models presented here.

As is apparent from equation 3, angular momentum is transported either by advection or viscous torques. For Keplerian rotation the viscous torque is given by

$$G = -3\pi \nu_i \Sigma R^2 \Omega_K, \quad (4)$$

where  $\nu_i$  is the kinematic viscosity.

Equations (3) and (2) can be combined (Pringle 1981) to give

$$\frac{\partial \Sigma}{\partial t} = \frac{3}{R} \frac{\partial}{\partial R} \left[ R^{1/2} \frac{\partial}{\partial R} \left( \nu_i \Sigma R^{1/2} \right) \right]. \quad (5)$$

We integrate this equation in time applying a zero-torque condition at the inner boundary ( $R_{\text{in}} = 3R_S$ , where  $R_S = 2GM/c^2$ ) and thus set  $\Sigma_{R_{\text{in}}=3R_S} = 0$ . At the outer boundary we feed the disc with a constant external accretion rate  $\dot{M}_{\text{ext}}$ . For advection we use a first-order donor cell upwind scheme. The integration conserves mass up to machine accuracy, accounting for mass supply at  $R_{\text{out}}$  and loss at  $R_{\text{in}}$ .

### 2.2 Radial force balance and hydrostatic equilibrium

We assume throughout that the disc is in hydrostatic equilibrium in the vertical direction (i.e. perpendicular to the disc plane). In the radial direction, the central gravitational pull is balanced by the centrifugal force

$$\Omega_K^2 R = \frac{GM}{R^2}. \quad (6)$$

The vertical structure is treated in the one-zone-approximation. Thus we take the vertical component of the gravitational force of the black hole to be balanced by the vertical pressure gradient, i.e.

$$\frac{\partial P}{\partial z} = -\rho g_z, \quad (7)$$

where  $g_z$  is the vertical gravity. In terms of our one-zone model we may write

$$\frac{\partial P}{\partial z} = P/H, \quad (8)$$

and

$$g_z = -\Omega_K^2 R \frac{H}{R}. \quad (9)$$

Using this, together with Equation 1 we obtain the relationship expressing vertical hydrodynamic equilibrium in the form

$$P = \frac{GM}{4\rho R^3} \Sigma^2. \quad (10)$$

### 2.3 Energy equation

We consider the heat content  $q$  of one half of an elemental disc annulus of width  $\Delta R$  at radius  $R$ , and height  $H$ . Then, from the

usual thermodynamic relations, and assuming hydrostatic equilibrium (Equation 10), we find (see Appendix A) that

$$\frac{dq}{dt} = \dot{e} + u_R \frac{\partial e}{\partial R} + AP\dot{H} + P \frac{\partial(2\pi R H u_R)}{\partial R}. \quad (11)$$

Here  $e$  is the internal energy of the semi-annulus, and the last two terms come from the ' $PdV$ ' work done on the semi-annulus.  $A = 2\pi R \Delta R$  represents the surface area of a disc annulus of width  $\Delta R$  at a given distance  $R$  from the black hole. The energy equation is then

$$\frac{dq}{dt} = A(Q^+ - Q^-). \quad (12)$$

The source terms on the RHS of the energy equation (11) are given by the viscous dissipation of the disc per unit annulus area,

$$Q^+ = \frac{9}{8} \nu_t \Sigma \frac{GM}{R^3}, \quad (13)$$

and radiative losses,  $Q^-$ , which we take to be of the form

$$Q^- = \frac{4\sigma}{3\tau} T^4, \quad (14)$$

where the optical depth  $\tau$  is given in terms of the opacity  $\kappa_R$  by

$$\tau = \frac{1}{2} \Sigma \kappa_R(\rho, T). \quad (15)$$

To ensure the consistency of the model we need disc to be optically thick in the vertical direction, i.e.  $\tau \gg 1$ .

We have written the numerical scheme so that internal energy  $e$  is conserved to machine accuracy, apart from losses on the inner and outer boundary and local source terms (i.e.  $PdV$ ). The boundary condition at the outer disc edge for the energy equation is taken to be divergence free, i.e. energy is being put in the last cell as it is lost to the next innermost cell. At the inner boundary energy is lost, assumed captured by the black hole.

## 2.4 Material functions

### 2.4.1 Equation of state

The total pressure  $P$  is given by the sum of gas and radiation pressure (since  $\tau \gg 1$ )

$$P = \rho \frac{k_B T}{\mu m_p} + \frac{4\sigma}{3c} T^4, \quad (16)$$

while the specific internal energy  $U$  of the mixture of monatomic gas & radiation is

$$U = \frac{3}{2} \frac{k_B T}{\mu m_p} + \frac{4\sigma}{c\rho} T^4. \quad (17)$$

The sound speed  $c_s$  can be calculated using

$$P = \gamma \rho c_s^2, \quad (18)$$

where the adiabatic index  $\gamma$  is given by

$$\gamma = \left( \frac{\partial \log P}{\partial \log \rho} \right)_s = \frac{16 - 12\beta_p - \frac{3}{2}\beta_p^2}{12 - \frac{21}{2}\beta_p}, \quad (19)$$

and is a slowly varying function of  $\beta_p$ , which ranges from  $\frac{4}{3}$  to  $\frac{5}{3}$  as  $\beta_p$  ranges from 0 to 1, where  $\beta_p$  is the ratio of gas pressure to total pressure.

### 2.4.2 Viscosity

We use the standard  $\alpha$ -viscosity prescription put forward by Shakura & Sunyaev (1973) and take the the  $(r\phi)$ -component of the stress tensor to be  $t_{r\phi} = -\alpha P$ . Relating this to the rate-of-strain tensor, through the viscosity  $\rho \nu_t$  (e.g. Bisnovatyi-Kogan & Lovelace 2001) so that  $t_{r\phi} = -\frac{3}{2} \nu_t \rho \Omega_K$  we see that the kinematic viscosity is related to  $\alpha$  by the equation

$$\nu_t = \frac{2}{3} \alpha \frac{P}{\rho \Omega_K}. \quad (20)$$

This viscosity prescription (eq. 20), using Eqns. (10), (1) and (18), can also be written in the form

$$\nu_t = \frac{2}{3} \alpha \sqrt{\gamma} c_s H. \quad (21)$$

If we envisage the viscosity  $\nu_t$  in physical terms as the product of a characteristic turbulent length and turbulent velocity,  $l_t$  and  $V_t$ , and our disc is assumed to be geometrically thin, we can associate the characteristic velocity and length scale with a fraction of the local scale height and of the local sound speed, respectively. In order that the turbulence remains subsonic we see that the factor  $2/3\alpha \sqrt{\gamma}$  needs to be smaller than, or of order, unity.

The viscous torque (4) using the viscosity prescription (20) can be written as

$$G = -4\pi\alpha P H R^2. \quad (22)$$

### 2.4.3 Opacity

We take the Rosseland mean opacity,  $\kappa_R$ , tabulated by the OPAL opacity project (Rogers & Iglesias 1992; Iglesias & Rogers 1996) for the solar composition of Grevesse & Noels (1993). We use the  $X = 0.7$  set of their opacity tables ( $X$  is the hydrogen mass fraction of the matter). Without further notice we fix the metallicity to be  $Z = 0.02$  (solar metallicity).

## 2.5 Numerical Grid and calculation procedure

We use a one-dimensional grid in radius with  $N$  points ranging from  $R_{\text{in}} = 3R_S$  to  $R_{\text{out}}$ . We solve the time-dependent equations (3), (2) and (11) using the mass  $m$  and internal energy  $e$  of a disc semi-annulus as dependent variables.

In order to allow simple application of the concepts of variable dynamo-driven angular momentum presented by King et al. (2004), it is necessary for the widths ( $\Delta R$ ) of the disc annuli to be comparable to the local disc thickness  $H$ . Within the context of the one-zone approximation, this is a reasonable assumption, since in this case it makes little physical sense to try to attribute physical reality to attempts at resolving structures significantly smaller than the scale height  $H$  of the disc.<sup>1</sup>

While  $R_{\text{in}}$  and  $R_{\text{out}}$  are kept constant, the number of grid-points is time-dependent and the number of grid points is adjusted according to the following prescription (see Fig. 1). We remove/insert grid points if the local radial extent of the annulus is larger/smaller than  $2H$  and  $0.5H$ , respectively. Grid points are inserted by conserving disc mass, angular momentum and energy  $e$ . In typical runs,  $N$  ranges between a few dozens and a few hundred points.

<sup>1</sup> Hameury et al. (1998) demonstrate that formal mathematical convergence of the numerical scheme may require a grid resolution much less than the disc thickness. We note here that mathematical convergence does not necessarily imply more accurate modelling of physical reality.

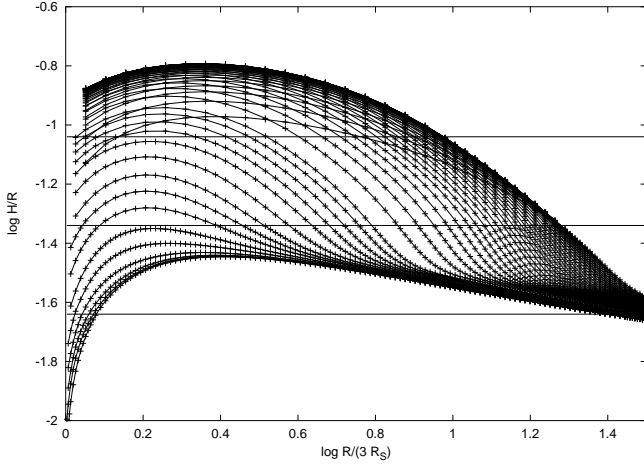


**Figure 1.** The refinement of the numerical grid. The Figure shows  $\log H/R$  versus  $\log R$  as it changes in a typical run. Every time the local scale height  $H$  exceeds (falls short of) twice (half) the local grid cell width, the resolution is reduced (increased). Due to the binarity requirement of the grid (see text) the same grid points are restored after repeated refinement/coarsening.

The setup of the grid is implemented as follows. At the start of the calculation there are 2 points, at  $R_{\text{in}}$  and  $R_{\text{out}}$ . Then we calculate the scale height  $H(R_{\text{out}})$  and compare it with the interval  $R_{\text{out}} - R_{\text{in}}$ . If  $R_{\text{out}} - R_{\text{in}} > 2H(R_{\text{out}})$ , we put a new grid point at  $R_{\text{new}} = \sqrt{R_{\text{out}}R_{\text{in}}}$  and calculate the scale height  $H(R_{\text{new}})$ . This procedure is recursively applied on both intervals. The setup is complete if there is no need to refinement any more.

From a numerical point of view it is beneficial in preventing numerical mixing to use a scheme which retains the structure of the grid cells fixed as far as possible. Thus, in order to maintain a binary structure of the grid (yielding the same coarse interval at the same place after several refinements), we assign each grid point with a number  $N$ , initially  $N(R_{\text{in}}) = 0$  and  $N(R_{\text{out}}) = 1$ . As a refinement occurs, the new grid point gets the mean number of the adjacent grid points. If this number is not an integer, all  $N$  are multiplied by 2. The condition of grid coarsening is accompanied by the condition for keeping the grid binary, i.e. we only remove a point if the  $N(R_{\text{outer}}) - N(R_{\text{remove}}) = N(R_{\text{remove}}) - N(R_{\text{inner}})$  and  $N(R_{\text{inner}})$  has to be an integer multiple of  $N(R_{\text{outer}}) - N(R_{\text{inner}})$ . This binarity of the grid ensures that, for example, the magnetic field is never mixed numerically across the entire grid, i.e. subsequent refinement and coarsening restores the same grid cell again.

A typical coarsening/refinement can be seen in Fig. 1. The  $\Delta(\log R)$  correlate very well with the  $H/R$  ratio since  $\Delta(\log R) = \log((R + \Delta R)/R) = \log(1 + \Delta R/R) \approx \Delta R/R = H/R$  as required. Every  $\Delta \log H/R = 0.3$  dex, i.e. at  $\log H/R \approx -1, -1.3$  and  $-1.6$  the resolution changes, as  $H$  de-/increases by a factor of 2.

## 2.6 Advection

It is often the case (see, for example, the discussion in Pringle et al. 1986) that the advective terms in the energy equation (i.e. those terms containing the radial velocity  $u_R$  on the RHS of Equation 11) are omitted. However, it was realised early that even in the case of dwarf nova discs these terms can make a difference (Faulkner et al. 1983). And more recently, Abramowicz et al. (1988) drew attention to the fact that the radial advection of heat can play an important role in the local energy balance in the disc, especially at high accretion rates close to the black hole, and can, in particular, have a

stabilising effect on the disc in that region. To illustrate this, we note that the terms responsible for the radial advection of energy can be written in terms of the radial entropy gradient as if they correspond to a local additional heat loss term (e.g. Muchotrzeb & Paczynski 1982; Bisnovatyi-Kogan & Lovelace 2001), in the form

$$Q_{\text{ad}} = \frac{\dot{M} T}{2\pi R} \frac{\partial S}{\partial R}. \quad (23)$$

The radial entropy gradient can be expanded in terms of pressure and radial density and temperature gradients. In doing so we obtain

$$Q_{\text{ad}} = \frac{\dot{M}}{2\pi R^2} \frac{P}{\rho} \chi_{\text{ad}}, \quad (24)$$

where the dimensionless measure of the strength of the effect,  $\chi_{\text{ad}}$ , includes the radial derivatives. Usually,  $\chi_{\text{ad}}(R)$  is a slowly varying function close to unity. However, although in the gas pressure dominated regime this value is indeed close to unity, in the radiation pressure dominated regime  $\chi_{\text{ad}}$  can be as large as 10,

Using the expressions for the internal energy and pressure in Appendix A, we can express  $\chi_{\text{ad}}$  in terms of the radial derivatives of  $\rho$  and  $T$  for a stationary disc

$$\chi_{\text{ad}} = - \left( 12 - \frac{21}{2} \beta_P \right) \frac{\partial \log T}{\partial \log R} + (4 - 3\beta_P) \frac{\partial \log \rho}{\partial \log R}. \quad (25)$$

## 3 STATIONARY SOLUTIONS AND STABILITY

Before investigating the time dependent disc behaviour, and before adding in the complications of stochastically driven accretion, we first investigate steady disc solutions, and the conditions for stability.

### 3.1 Stationary solutions

In the stationary case, with accretion rate  $\dot{M} = \text{const.}$ , we have  $\partial/\partial t = 0$  and thus the conservation of angular momentum (Eqn. 3) becomes

$$\dot{M} f = 3\pi v_i \Sigma, \quad (26)$$

conservation of energy (11) becomes

$$Q^+ - Q^- - Q_{\text{ad}} = 0, \quad (27)$$

and vertical hydrostatic equilibrium (10) remains

$$P = \frac{GM}{4\rho R^3} \Sigma^2, \quad (28)$$

where the function  $f(R) = 1 - (R/R_{\text{in}})^{1/2}$  ensures compliance with the inner boundary condition. For a given accretion rate, and at a particular radius, these three equations can be written as two equations, depending on pressure  $P$ , density  $\rho$  and temperature  $T$ . The energy equation yields

$$\frac{\dot{M}}{2\pi R^2} \left( \frac{3}{4} \Omega_K^2 R^2 f - \frac{P}{\rho} \chi_{\text{ad}} \right) - \frac{16\pi\sigma T^4 \alpha P}{3\kappa_R \rho \Omega_K \dot{M} f} = 0, \quad (29)$$

and hydrostatic equilibrium yields

$$P^3 - \frac{\Omega_K^4 \dot{M}^2 f^2 \rho}{16\pi^2 \alpha^2} = 0. \quad (30)$$

Then for a given accretion rate, and at a particular radius, these two equations, together with the equation of state (Equation 16) can be solved for  $P$ ,  $\rho$  and  $T$ .

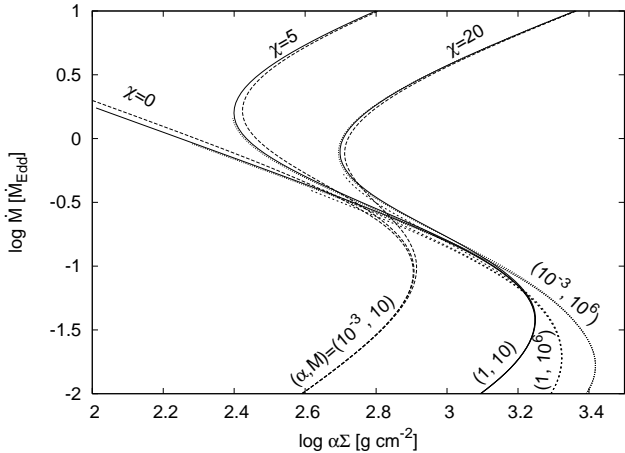


**Figure 2.** Local equilibrium solutions at  $R = 30R_S$  for a range of accretion rates. We consider solutions for different values of viscosity parameter  $\alpha$ , the black hole mass  $M$  and the strength of radial advection,  $\chi_{\text{ad}}$ . Parts with negative  $\dot{M} - \Sigma$  slope are thermally and viscously unstable. Note the stabilising effect of advection (when  $\chi_{\text{ad}} \neq 0$ ).

We solve these equations with a 2D nested-intervals method as described in Mayer & Duschl (2005). In general we consider the conditions at a particular radius  $R$ , for various values of the accretion rate  $\dot{M}$ . For illustrative purposes we also consider the solutions for three different particular values of the strength of the adiabatic heat flux  $\chi_{\text{ad}}$ , and for various values of the viscosity parameter  $\alpha$ .

We present our results in terms of the Eddington luminosity and the corresponding Eddington accretion rate. In terms of the Eddington luminosity,  $L_{\text{Edd}} = 4\pi GMm_p c / \sigma_T$  we may define a corresponding Eddington accretion rate by

$$L_{\text{Edd}} = \eta_K \dot{M}_{\text{Edd}} c^2, \quad (31)$$

where  $\eta_K$  is the efficiency. For a typical value of  $\eta_K = 1/12$  (see below) we find in numerical terms

$$\dot{M}_{\text{Edd}} = 2.68 \cdot 10^{-7} \cdot \left( \frac{M}{10M_{\odot}} \right) M_{\odot} \text{yr}^{-1}. \quad (32)$$

### 3.2 S-Curves

In Fig. 2 we plot the relationship between accretion rate  $\dot{M}$  and  $\alpha$  times disc surface density  $\Sigma$  for different values of radially constant  $\alpha$  and for different values of  $\chi_{\text{ad}}$  and of the central mass  $M$ .

These plots give us direct information about the stability of the steady-state discs. There are two types of instability which these discs can be subject to – viscous (e.g. Lightman & Eardley 1974) and thermal (Pringle 1976). We show in Appendix B that the stability criterion in both cases is the same. The discs are unstable when

$$\left( \frac{\partial \log \dot{M}}{\partial \log \Sigma} \right)_{p,T} < 0. \quad (33)$$

From Figure 2 we see that in the absence of heat advection the discs become unstable (i.e. the  $\dot{M}(\Sigma)$  curves have negative gradient) as the accretion rates approach the Eddington limit. But, as pointed out by Abramowicz et al. (1988), advection of heat (i.e. non-zero  $\chi_{\text{ad}}$ ) provides stability. For all combinations of  $\alpha$  and  $M$  considered, we see that within the physical range for  $\chi_{\text{ad}}$  there are always values of the accretion rate for which the discs are unstable, whereas for

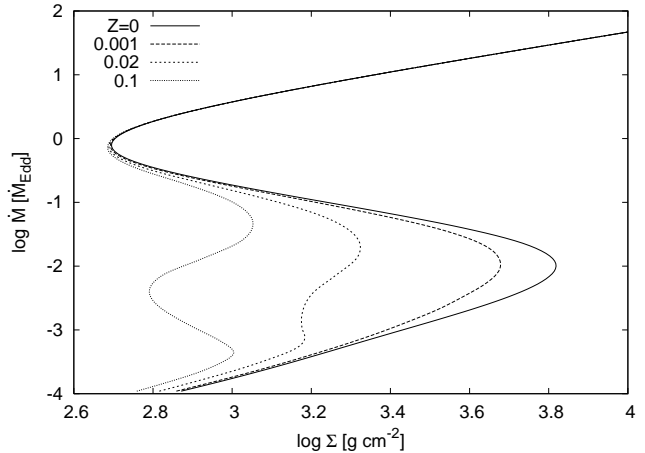


**Figure 3.** Local equilibrium solution at  $R = 30R_S$  for  $M = 10^6 M_{\odot}$ ,  $\alpha = 1$ ,  $\chi_{\text{ad}} = 20$  and different metallicities  $Z = 0, 0.001, 0.02$  (solar) and  $Z = 0.1$ . The hydrogen content is fixed at  $X = 0.7$ .

higher black hole mass  $M$ , higher  $\alpha$  and lower  $\chi_{\text{ad}}$  the range of accretion rates we get instability becomes larger.

It is well known (see, for example, Lasota 2001) that the instability causes the disc to undergo limit-cycle behaviour. We investigate this further below.

### 3.3 Dependency on black hole mass and metallicity

For black hole masses typical of X-ray binaries ( $M \approx 10 M_{\odot}$ ), characteristic mid plane temperatures close to the black hole are of the order of  $10^7$  K.

Since  $\dot{M}\Omega_K^2 \propto T^4/\tau_R$  (cf. eq. 27) in the absence of advection, we get in scaled units ( $R$  in Schwarzschild Radii,  $\dot{M}$  in units of Eddington accretion rate) and roughly constant optical depth that  $T \propto M^{-1/4}$ . For a black hole mass of  $10^6 M_{\odot}$  we then expect the mid plane temperature of the disc to be of the order of a few times  $10^5$  K.

For  $10^6 M_{\odot}$  the disc temperature reaches  $T \approx 10^{5.4}$  K for reasonable accretion rates. Then the disc shows an additional instability caused by the “Z-Bump” (cf. Seaton et al. 1994) in the opacity for a metallicity larger than  $Z = 0.02$ . This so called Z-Bump is also responsible for pulsations in  $\beta$  Cep stars (Simon 1982; Kiriakidis et al. 1992). We show a S-curve presenting this instability in Fig. 3. It is evident that the disc for this instability locally can jump from accretion rates of  $10^{-4} \dots 10^{-3}$  to  $10^{-1} M_{\text{Edd}}$ .

Generally, the disc becomes more unstable with increasing mass of the black hole, i.e. the lower turning point in the “S-curve” moves to lower accretion rates.

### 3.4 H/R in the presence of advection

For the approximations used in this paper to be valid we require that the disc thickness be small compared to the radius. We note here that the addition of a local heat sink in the guise of advection implies that the disc is typically thinner than it would be if all the energy generated locally were radiated at the same radius. In the stationary case, when advection of heat strongly dominates radiative losses (so that  $Q_{\text{ad}} \gg Q^-$ ), Equation (29) becomes

$$\frac{3}{4} (\Omega_K R)^2 f - \frac{P}{\rho} \chi_{\text{ad}} = 0. \quad (34)$$

Then using hydrostatic equilibrium (Equation 10) we find that

$$\frac{H}{R} = \sqrt{\frac{3f}{4\chi_{\text{ad}}}}. \quad (35)$$

Thus, for example, taking  $\chi_{\text{ad}} = 10$  as a representative value, and with  $f = \frac{1}{2}$  (corresponding to  $R \approx 10R_{\text{g}}$ ) we find  $H/R \approx 0.2$ . Indeed, we see that as long as  $\chi_{\text{ad}} > 4/3$ ,  $H/R$  is smaller than unity.

### 3.5 Keplerian rotation

For similar reasons, if advective heat flow is important, the disc angular velocity stays close to Keplerian. If we include the radial pressure gradient in the radial momentum balance equation, we find that the disc angular velocity  $\Omega$  is given by

$$\Omega^2 = \frac{GM}{R^3} \left( 1 + \frac{PR}{GM\rho} \xi_P \right), \quad (36)$$

where

$$-\xi_P = \frac{\partial \log P}{\partial \log R}. \quad (37)$$

This may be written as

$$\xi_P = \beta_P \frac{\partial \log \rho}{\partial \log R} + (4 - 3\beta_P) \frac{\partial \log T}{\partial \log R}. \quad (38)$$

The dominant term in the radiation pressure dominated domain ( $\beta_P = 0$ ) is, of course, the temperature gradient, and a representative value is  $\xi_P \approx 2$ .

In (36) we treat the extra term in the brackets as small deviation. Thus we can replace  $GM/R$  by  $(\Omega_{\text{K}}R)^2$  and with the hydrostatic equilibrium (10) we get

$$\Omega^2 = \Omega_{\text{K}}^2 \left( 1 + \left( \frac{H}{R} \right)^2 \xi_P \right). \quad (39)$$

When advective heat transport is strongly dominant we can use Equation (35) to deduce that

$$\Omega^2 = \Omega_{\text{K}}^2 \left( 1 + \frac{3f\xi_P}{4\chi_{\text{ad}}} \right). \quad (40)$$

For small deviation ( $\Omega - \Omega_{\text{K}} \ll \Omega_{\text{K}}$ ) this gives approximately

$$\frac{\Omega}{\Omega_{\text{K}}} - 1 = \frac{3f\xi_P}{8\chi_{\text{ad}}}. \quad (41)$$

Thus, using representative values, the deviation from Keplerian rotation when advective heat transport is strong never exceeds around 4 per cent. The assumption of Keplerian rotation is therefore a reasonable one.

## 4 TIME-DEPENDENCE - RESULTS

We have seen above that even in the absence of stochastic magnetic phenomena our accretion disc models are expected to display time-dependent behaviour for some ranges of the parameters. We have carried out a number of simulations for different values of  $\alpha$ , different external (or mean) accretion rates and different black hole masses.

In this section, for reasons of computational time, we use a logarithmically equidistant grid with  $N = 500$  grid points without refinement and coarsening. We solve the equations with an implicit solver. Comparison with the standard explicit solver and the refinement and coarsening as described in Sect. 2.5 does not show significant deviations. However the computing time decreased drastically

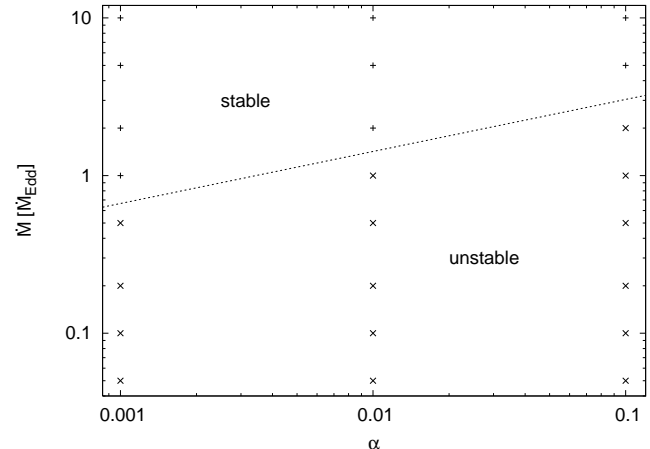


**Figure 4.**  $\dot{M}$  versus  $\alpha$  showing the systems with limit cycles (to the lower right of each line) and without (upper left) for a  $10 M_{\odot}$  black hole. The line is only a rough indication since the grid in  $(\dot{M}, \alpha)$  is very coarse. The points, for which actually calculations have been done, are indicated by the crosses.

and thus enabled us to carry out a parameter study concerning the global stability of these discs with respect to the instabilities discussed above.

### 4.1 General behaviour

Our time-dependent models depend on the mass of the black hole, the external accretion rate and the value of the viscosity parameter  $\alpha$ .

As initial conditions we set up a stationary disc, assuming  $Q^+ = Q^-$  and neglecting advection. Depending on the accretion rate and the viscosity parameter, the disc either continues to stay in this stationary state, or, if advection of heat is important, the inner disc re-adjusts itself to allow for the advection. As we see from Figure 2 if the viscosity is high enough, we expect limit cycles to appear with the inner disc oscillating between a hot state with high accretion rate and a cool state with lower accretion rate (see Section 3.2).

If the inner disc is such that the mean accretion rate produces instability, the inner disc spends its time trying to jump between the two stable branches of the S-curve. While it is on the upper branch, with advection important, the disc is steadily depleted. The surface density decreases while the accretion rate is higher than average. As the inner disc is depleted, some matter is transported outward in a heating front. The inner disc is radiation pressure dominated and the accretion rate there is radially constant. Matter then piles up ahead of this front and subsequently the inner disc begins to starve and the accretion rate decreases. When the front reaches the stable, gas pressure dominated region of the disc, the front slows down and the inner disc cools, becoming more gas pressure dominated, as the supply of matter is interrupted. The dissipated energy is advected outwards and the accretion rate in the inner disc decreases, varying radially as  $\dot{M} \propto R^2$ . Then inner disc reheats, the accretion rate increases inwards, the pileup is accreted and eventually the cycle restarts with the inner disc again becoming depleted.

## 4.2 Influence of $\alpha$ and the black hole mass on the stability

The parameters for the grid of models with constant  $\alpha$  discs we ran are shown in Figure 4 for a  $10 M_{\odot}$  black hole. Also shown in Figure 4 are those parameter values for which limit-cycle behaviour is found. The higher the viscosity parameter, the more unstable the disc becomes since then advection can only stabilise for higher accretion rates.

For higher black hole masses, there are several complications. First, the radiation pressure dominated zone and hence the Lightman & Eardley (1974) unstable region is larger. For  $10^7 M_{\odot}$  this zone is so large (more than 1000 Schwarzschild radii), that there is likely to be an interaction between this instability and the usual dwarf nova instability, caused by the opacity drop at hydrogen ionisation. This has yet to be explored (cf. Clarke 1988; Clarke & Shields 1989).

Second, as discussed previously, there is a "Z-Bump" instability present which makes the results extremely dependent on the chosen metal content for the opacity.

Finally the computational effort becomes increasingly larger. The disc in the Lightman & Eardley (1974) unstable region oscillates between a thick disc and a more and more ultra-thin disc ( $H/R \approx 10^{-4} \dots 10^{-3}$ ) which puts strong limits on the time-step.

These restrictions led us to concentrate on the  $10 M_{\odot}$  black hole case and to leave the higher mass case for further investigations. We plot a sample lightcurve and a power density spectrum for a  $10^6 M_{\odot}$  black hole in Fig. 7. The two different instabilities (Lightman & Eardley 1974, and the "Z-Bump" instability) operate on different timescales and different amplitudes. The Lightman & Eardley (1974) instability leads to the huge outbursts in luminosity, while the small fluctuations are due to the "Z-Bump" instability. For the example chosen this instability affects only the region around 100 Schwarzschild radii. The instability then only appears as small fluctuations in the total disc luminosity. Note that for computational feasibility we set the number of grid points artificially low. In order to fulfil our resolution criterion ( $\Delta R \approx H$ , cf. Sect. 2.5), we would have needed  $N \approx 3000$  points to properly resolve the inner disc in the low- $\dot{M}$  state. Thus the lightcurve is only indicative of the complications that can occur.

## 4.3 Effect of advection on the observed accretion rate

By definition the radiative luminosity of the disc is

$$L_{\text{rad}} = 2\pi \int_{R_{\text{in}}}^{R_{\text{out}}} Q^- R dR. \quad (42)$$

For an infinitely extended, steady standard disc ( $R_{\text{out}} \rightarrow \infty$ , no radial advection of heat), the energy dissipated in the disc by viscous processes (using our inner 'black hole' radius  $R_{\text{in}} = 3R_S = 6GM/c^2$ ) is

$$L_{\text{diss}} = \frac{1}{2} \frac{GM\dot{M}}{R_{\text{in}}} = \frac{1}{12} \dot{M}c^2. \quad (43)$$

Thus the efficiency  $\eta_K$  of our Newtonian, standard black hole accretion disc in Keplerian rotation extending from  $R_{\text{in}} = 3R_S$  to infinity in converting rest mass energy into radiation is  $\eta_K = \frac{1}{12}$ .

In the absence of advective heat flow, for an assumed value of the efficiency  $\eta_K$  a measurement of the observed radiative flux, i.e.  $L_{\text{rad}}$ , yields an estimate of the accretion rate by setting  $L_{\text{rad}} = L_{\text{diss}}$ . However, when advection of heat is important, we expect deviations from the standard  $L_{\text{rad}} \propto \dot{M}$  relation. In particular, since some of the dissipated heat is now advected directly into the black hole,

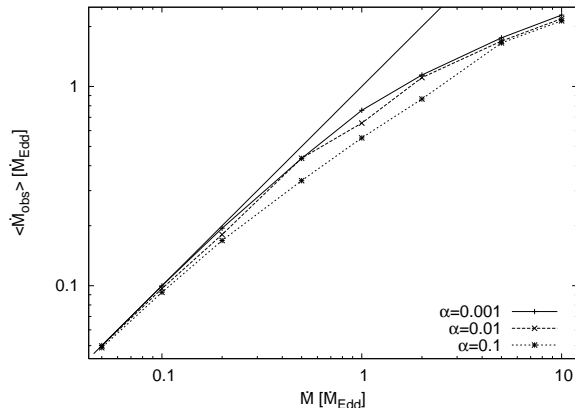


**Figure 5.** The time-averaged 'observed' accretion rate,  $\dot{M}_{\text{obs}}$ , deduced from the radiative luminosity  $L_{\text{rad}}$ , is plotted versus the external (actual) accretion rate  $\dot{M}$  for a  $10 M_{\odot}$  black hole for different values of  $\alpha$ . For high actual accretion rates, some of the accretion energy is advected into the black hole.

we expect the observed radiated flux to give an underestimate of the actual accretion rate. From the numerical simulations, we calculate the radiative luminosity  $L_{\text{rad}}(t)$  at a given time, and deduce from an 'observed' accretion rate given by

$$\dot{M}_{\text{obs}}(t) = \frac{L_{\text{rad}}(t)}{\eta_K c^2}, \quad (44)$$

or the time-average of this

$$\langle \dot{M}_{\text{obs}} \rangle = \frac{1}{\eta_K c^2 T} \int^T L_{\text{rad}}(t) dt. \quad (45)$$

In Fig. 5 we plot  $\langle \dot{M}_{\text{obs}} \rangle$  versus the actual accretion rate  $\dot{M}$ , both in units of the Eddington accretion rate. If the disc model at the given set of parameters shows limit-cycle behaviour, we calculate the time-averaged value of  $L_{\text{rad}}$  for an integer number of complete limit cycles.

For a  $10 M_{\odot}$  black hole at low accretion rates, we find as expected  $\langle \dot{M}_{\text{obs}} \rangle = \dot{M}$ . With increasing accretion rate, however, the advection comes into play and the "observationally calculated" accretion rate deviates from the actual  $\dot{M}$ . For a  $10 M_{\odot}$  black hole this relation is practically independent of  $\alpha$ . This deviation may be related to the deviations from the  $L_{\text{rad}} \propto T_{\text{in}}^4$  relationship recently reported by Kubota & Makishima (2004) and Abe et al. (2005). They find the so called 'apparently standard' regime in observations of XTE J1550-564 and 4U 1630-47, where the disc luminosity is proportional to  $T_{\text{in}}^2$  and attribute this to effects of the radial advection of energy.

For the  $10^6 M_{\odot}$  black hole (Fig. 7). There are departures from  $\langle \dot{M}_{\text{obs}} \rangle = \dot{M}$ . While the disc is being fed with an accretion rate of  $\dot{M} = 0.1 \dot{M}_{\text{Edd}}$ ,  $\langle \dot{M}_{\text{obs}} \rangle$  is only 44 % of the actual accretion rate, while the time average for the low- $\dot{M}$  state only is as low as 1.5 % of the actual accretion rate. This is a result of the strong outburst behaviour of these discs compared to the low-mass case. Most of the mass previously stored in the outer disc is pushed through the inner disc in the high- $\dot{M}$  state. Then, however, most of the energy created by viscous dissipation is advected into the black hole. Since the outbursts are short compared to the complete limit cycle, the efficiency is fairly low.

#### 4.4 Power density spectra

We calculate lightcurves at equidistant time points. Suppose we have a lightcurve covering the time  $T$  with  $N$  points. We calculate power density spectra using the canonical normalisation to get the Power  $P_\nu$  in units of  $(\text{rms}/\text{mean})^2/\text{Hz}$ . Integrating  $P_\nu d\nu$  gives the integrated fractional rms. We compute the FFT of the lightcurve and then define  $P_\nu$  by (Lewin et al. 1988)

$$P_\nu = \frac{2|a_\nu|^2}{\bar{L}^2 T} \left(\frac{T}{N}\right)^2 \quad (46)$$

where  $\bar{L}$  is the mean luminosity of the lightcurve and  $a_\nu$  the non-normalised Fourier coefficient. The  $P_\nu$ 's are binned into logarithmically equidistant points. For the FFT we use the routines from the FFTW library<sup>2</sup>.

The integrated fractional rms is given in percent

$$r = 100\% \cdot \sqrt{\int P_\nu d\nu} \quad (47)$$

Using Parseval's theorem, it can be shown, that  $r$  indeed corresponds to the rms/mean of the luminosity fluctuations

$$r = 100\% \cdot \sqrt{\frac{1}{N} \sum_{i=1}^N \left(\frac{L_i}{\bar{L}} - 1\right)^2} \quad (48)$$

where  $L_i$  is the luminosity given at equidistant time intervals and  $\bar{L}$  the time-average of the total light curve. Unless otherwise stated, the last formula is used to calculate the integrated fractional rms.

#### 4.5 Period of limit cycle

A sample lightcurve and power spectrum for a  $10 M_\odot$  black hole is shown in Fig. 6. We binned the FFT data in logarithmically equispaced bins of width  $\Delta\nu/\nu = 0.005$ . The disc undergoes limit cycles on a timescale of roughly 600 s. Note that besides the fundamental frequency and their higher harmonics there are more peaks present. These arise from the asymmetry of the lightcurve.

The luminosity of the disc is given in terms of  $\dot{M}_{\text{obs}}/\dot{M}$ , where  $\dot{M}$  is the external/average accretion rate and  $\dot{M}_{\text{obs}}$  the "observed" accretion rate. This ratio is equivalent to the ratio between the actual luminosity and the luminosity of a stationary disc where no advection is taken into account.

## 5 COMPARISON WITH PREVIOUS WORK

In this Section we briefly compare our models with previous and recent work in the field. We restrict ourselves to optically thick disc models.

There is no absolutely correct way of doing 1D accretion disc models in the one-zone approximation, and in this paper we have adopted the simplest approach, by ignoring all the details of the vertical structure. To do it properly clearly requires doing two-dimensional hydrodynamics. In Appendix A we derive the LHS of the energy equation (11) explicitly from first principles. We work in terms of the total internal energy and the mass of a disc annulus. All other variables can be expressed in terms of mass and internal energy of a disc annulus.

In early work on black hole accretion discs, Honma et al. (1991) presented disc models with an energy equation containing

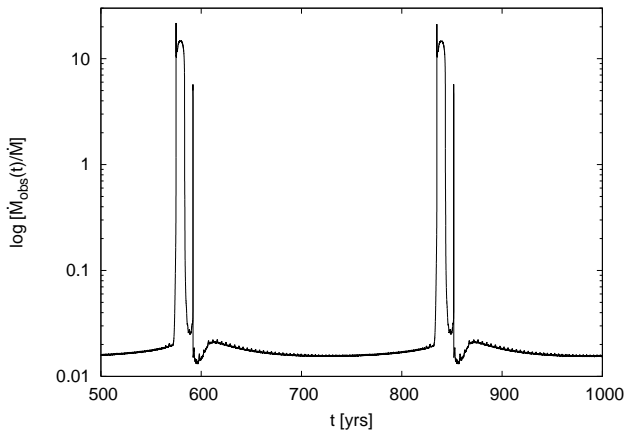


**Figure 7.** Lightcurve for an accretion disc around a  $10^6 M_\odot$  black hole accreting at  $0.1 \dot{M}_{\text{Edd}}$ .  $\alpha = 0.1$ . The metallicity is  $Z = 0.1$ , the number of grid points has been set to  $N = 250$ . Note that the lightcurve resembles the instabilities present in Fig. 3.

the evolution of the total energy. They apply correction factors to try to take account of details of the vertical disc structure. They mainly consider  $M = 10 M_\odot$  and  $\alpha = 0.1$  but make use of a modified " $\alpha$ - $P$ "-description by multiplying the  $r\phi$ -component of the viscous stress-tensor with a factor  $\beta_p^l$ . (Here  $\beta_p$  is the ratio of gas pressure related to total pressure, so that  $q = 0$  corresponds to what we use here, and  $q = 1$  corresponds to the  $r\phi$ -component being proportional to  $\alpha P_{\text{gas}}$ .) For  $q \geq 0.5$  they find stable disc solutions while for  $q < 0.5$  they find limit-cycle solutions of increasing amplitude. Their  $q = 0$  results are compatible with ours.

In a series of papers Szuszkiewicz & Miller (1997, 1998, 2001) take a similar approach to Honma et al. (1991) except that they use different numerical factors to try to take account of the details of the vertical disc structure. For this reason, while their results are in line with those of Honma et al. (1991) and those presented here, they differ in some minor details. In particular, they find unstable solutions for a  $10 M_\odot$  black hole and  $\alpha = 10^{-3}$  for  $0.09 < L_{\text{Edd}} < 1$  which is in line with our models except the high- $\dot{M}$  end, where we find stability at  $1 L_{\text{Edd}}$ . They subsequently develop a scheme where they take account of the possibility that the disc might become optically thin and there is non-Keplerian rotation.

Nayakshin et al. (2000) present a model with the specific application to GRS1915+105. They additionally include thermal and radiation diffusion in radial direction. For the simulations presented in this paper, however, these terms never become important. They might become comparable to the terms containing the radial advection of the internal energy, but this only will result in factors of two at most. In the context of working in the one-zone-approximation, the omission of these terms in our simulations seems to be justified. They investigate models with different radially varying values for the viscosity parameter  $\alpha$ . They furthermore try to account for additional cooling in a corona and include some flickering. Their flickering is a random ad-hoc modulation of the efficiency of radiation coming from the inner parts of the disk. Lightcurves similar to GRS1915+105 can be produced. No further diagnostics of the flickering process (i.e. power density spectrum) are tested there.

Janiuk et al. (2002) consider a similar approach to the one presented in this paper. They write the change in specific heat in terms of temperature and density (i.e. surface density and scale height, setting the radial advection of the scale height to zero). They apply yet another set of correction factors to try to take account of the

<sup>2</sup> <http://www.fftw.org/>



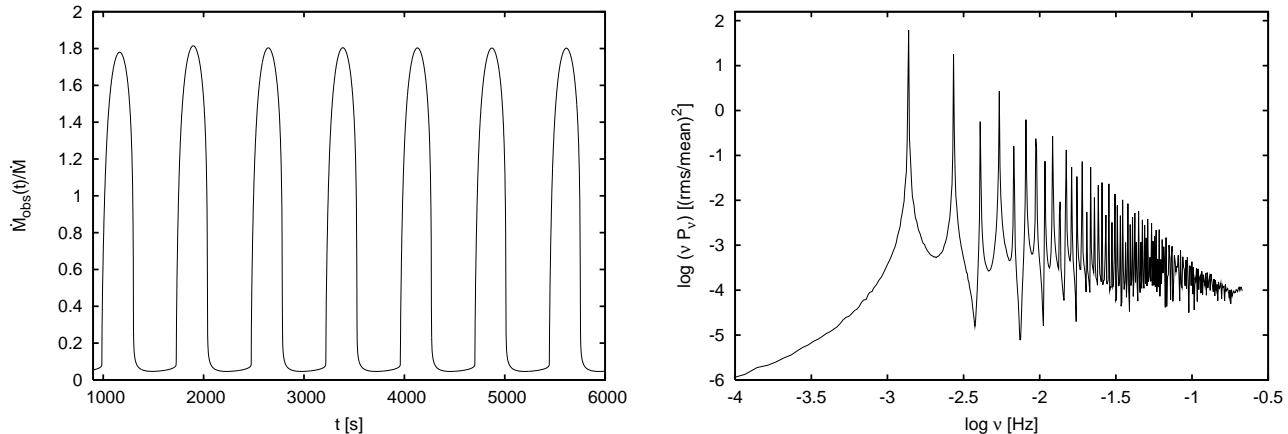


**Figure 6.** (left) Lightcurve (detail) and (right) Power density spectrum for an accretion disc around a  $10 M_{\odot}$  black hole accreting at  $0.5 \dot{M}_{\text{Edd}}$ .  $\alpha = 0.1$ . The FFT data are binned in logarithmically equispaced bins of width  $\Delta\nu/\nu = 0.005$ .

vertical structure. Their results are in line with those obtained by Szuszkiewicz & Miller (1997, 1998, 2001).

In conclusion, these various approaches differ mainly in the nature and actual numerical values of the correction factors (being in the range 0.2 – 16) applied when trying to take some account of the vertical disc structure. There seems to be no unanimity on the values that should be applied. In this paper we have taken the simple approach of setting all these factors to unity.

Some of the work reviewed here (Nayakshin et al. 2000; Janiuk et al. 2002) also include prescriptions for energy loss to a wind. While there is agreement that mass loss does not influence the results, energy loss (cooling) does influence the disc and stabilises it. Energy loss usually is only parametrised with a fraction of the radiative losses taken away to the corona or the wind. This fraction is either set constant or depends on the accretion rate (e.g. Janiuk et al. 2002). Without the energy loss to a wind, our results so far are in agreement with the results in literature.

In the next section we shall introduce our model for the flickering which contains a self-consistent coupling between the mass, energy and angular momentum loss of the disc to a wind coupled to the physical model for the flickering.

## 6 THE MODEL FOR THE FLICKERING

### 6.1 The basic mechanism

We now address the means of introducing a physical mechanism to produce the observed short-timescale variability in black hole accretion discs. As we mentioned in the Introduction the main problem is to find a mechanism which gives the right amplitude and the right timescale.

Lyubarskii (1997) showed that if the viscosity parameter  $\alpha$  changes in a spatially uncorrelated manner on the local viscous timescale at each radius, then the characteristic flickering spectrum and the long timescales can be produced, but was unable to suggest a physical mechanism which would produce this result. King et al. (2004), following Livio et al. (2003), put forward a solution. The main problem is that local variations in  $\alpha$  are correlated with small variations in the disc's internal magnetic field which is generated by a local disc dynamo. This operates characteristically on about the local dynamical timescale. They envisage the disc dynamo operating as a set of essentially independent dynamo cells with char-

acteristic radial width comparable to the local disc thickness. They then propose that the dynamo mechanism also gives rise to a small poloidal field in each cell. Most of the time this local poloidal flux is randomly aligned from cell to cell and so has no net effect. But from time to time this poloidal field magnetic field is sufficiently aligned from cell to cell that it gives rise to a large scale magnetic field which is able to generate an outflow (wind or jet) which removes angular momentum from the disc. Since the local field in each dynamo cell changes on about the local dynamical timescale, this overall alignment only happens on a large multiple of the dynamical timescale and thus can be comparable or even longer than the viscous timescale.

We now apply these ideas to the thermal disc structure developed above. We stress here the additional concepts required in applying this model to a realistic disc. More details of the underlying ideas can be found in King et al. (2004). In the following subsections we describe the details of this model and the equations involved.

### 6.2 Evolution of the poloidal magnetic field

We consider a poloidal magnetic field  $B_z$  which evolves according to the induction equation

$$\frac{\partial B_z}{\partial t} = \frac{1}{R} \frac{\partial}{\partial R} \left( R \eta^* \frac{\partial B_z}{\partial R} \right) - \frac{1}{R} \frac{\partial}{\partial R} (R B_z U_R) + S_B. \quad (49)$$

We allow the field to diffuse radially with an effective magnetic diffusivity  $\eta^*$  and allow for radial advection at velocity  $U_R$  which is due to a magnetic wind torque.  $S_B$  stands for a source term for the poloidal field which is assumed to be generated by the local magnetic dynamo. At the outer disc boundary we take  $B_z = 0$ , allowing magnetic flux to diffuse outwards, but preventing inward flux advection.

### 6.3 The source of poloidal field, $S_B$

The poloidal field  $B_z$  is assumed to be generated by the disc dynamo which generates the main disc viscosity. The magnetic field in the disc, partitioned into disc annuli of radial extent  $\Delta R \approx H$ , is assumed to change independently in each dynamo cell in a stochastic fashion on the characteristic dynamo time scale

$$\tau_d = k_d \Omega_K^{-1}, \quad (50)$$

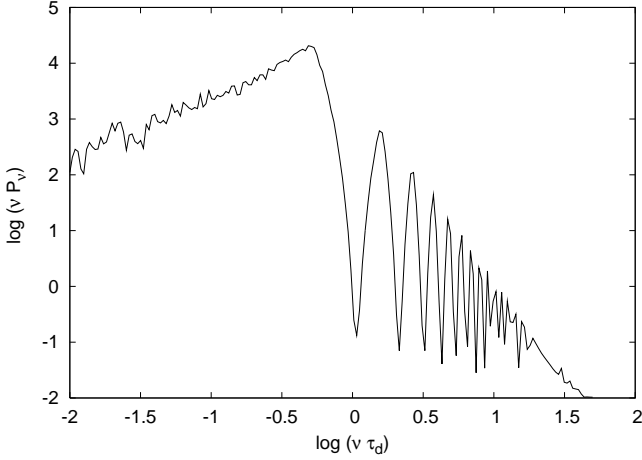


**Figure 8.** The power spectrum is shown for a sample time-series of a Markoff chain series (see eq. 53) for  $\alpha_1 = 0.5$ . This series is used to mimic the effects of locally acting magnetic dynamos. In this figure we show the power spectrum for a dynamo acting on a timescale  $\tau_d$ . To account for timescales smaller than  $\tau_d$ , we linearly interpolated the Markoff chain. The frequency is normalised to  $\tau_d$ . The peak at the dimensionless frequency  $\log(v\tau_d) = 0$  is clearly visible including higher harmonics. Most of the power is released on slightly longer timescales (approximately  $2.5\tau_d$ ) coming from the broad peak at  $\log(v\tau_d) \approx -0.4$ .

which we take to be a multiple of the local dynamical time scale (we take  $k_d = 10$ , cf. Tout & Pringle 1992; Stone et al. 1996)

Each annulus of the disc is assumed to generate a sufficiently large internal tangled magnetic field of strength  $B_{\text{disc}}$  which generates the effective disc viscosity with  $\alpha$  parameter (Shakura & Sunyaev 1973)

$$\alpha = \frac{B_{\text{disc}}^2}{4\pi P}. \quad (51)$$

Although we assume that each dynamo cell generates a local poloidal field  $B_z$ , we expect the magnitude of the poloidal component to be small. We define a parameter  $\beta_s$  so that the maximum value of the poloidal field,  $B_{z,\text{max}}$  is given by

$$B_{z,\text{max}} = \beta_s B_{\text{disc}}, \quad (52)$$

where  $B_{\text{disc}}$  is given by Equation 51. We expect  $\beta_s \ll 1$ .

We then model the stochastic nature of the local poloidal field in the following way. At each radius we define a set of times,  $t_n = n\tau_d$ ,  $n = 1, 2, \dots$  as integral multiples of the local dynamo timescale at which the field changes. At each of these times we generate a random number,  $u(t_n)$ , according to the Markoff process

$$u(t_{n+1}) = -\alpha_1 u(t_n) + \epsilon(t_n), \quad (53)$$

where  $\epsilon(t_n)$  is a random variable of zero mean and unit variance, and we take  $\alpha_1 = 0.5$ . The new value of the magnetic field strength in the disc annulus then is given by

$$B_z(t_{n+1}) = u(t_{n+1}) B_{z,\text{max}}. \quad (54)$$

We show a power spectrum of a sample time-series for  $u(t_n)$  for a magnetic dynamo acting locally on the dynamo time scale  $\tau_d$  in Fig. 8. For the purposes of the Figure, in order to resolve shorter timescales than the dynamo timescale, we applied a linear interpolation between the timesteps. We note that the power spectrum peaks at a period of a few times  $\tau_d$ .

As mentioned above, in order to ensure the consistency of the model, we need to make sure that the poloidal field  $B_z$  is always

smaller than the disc magnetic field. This implies  $\beta_s^2 \ll 1$ , so that energetically the poloidal field is negligible. Thus this assumption furthermore allows us to neglect the energy generation/loss due to our dynamo process. Tout & Pringle (1996) estimate this fraction to be  $\sim H/R$ .

#### 6.4 Magnetic torque and the wind

We assume that angular momentum loss occurs due to a magnetic wind/jet when the poloidal field is of sufficiently large scale. This is likely to occur when the poloidal fields generated by the individual dynamo cells are, by chance, spatially correlated over a radial extent of the order of  $R$ . To measure the degree of spatial correlation in the simulation, we define the radial averages

$$\langle B_z \rangle = \frac{\int_{R-\Delta^-}^{R+\Delta^+} B_z R dR}{\int_{R-\Delta^-}^{R+\Delta^+} R dR}, \quad (55)$$

$$\langle B_z^2 \rangle = \frac{\int_{R-\Delta^-}^{R+\Delta^+} B_z^2 R dR}{\int_{R-\Delta^-}^{R+\Delta^+} R dR}. \quad (56)$$

We choose the total interval over which we measure the correlation as equal to  $R$ , that is we take

$$\Delta^- + \Delta^+ = R. \quad (57)$$

We then choose  $R$  to be the geometric mean of  $R - \Delta_-$  and  $R + \Delta_+$ . Thus we choose the dimensionless constant  $a$  so that  $R - \Delta^- = R/a$ ,  $R + \Delta^+ = aR$  with  $a > 1$ . This then implies that  $a = (1 + \sqrt{5})/2$ , the golden ratio.

Thus we obtain

$$\langle B_z \rangle = \frac{\int_{R-\Delta^-}^{R+\Delta^+} B_z R dR}{R^2 (a^2 - 1/a^2)}, \quad (58)$$

$$\langle B_z^2 \rangle = \frac{\int_{R-\Delta^-}^{R+\Delta^+} B_z^2 R dR}{R^2 (a^2 - 1/a^2)}, \quad (59)$$

where we note that  $a^2 - 1/a^2 = \sqrt{5}$ .

We now define the quantity

$$Q = \frac{\langle B_z \rangle^2}{\langle B_z^2 \rangle}, \quad (60)$$

which represents the degree of spatial correlation of the poloidal magnetic field in neighbouring disc annuli. We note that  $0 \leq Q \leq 1$ , where  $Q = 1$  represents a fully coherent magnetic field, while for  $Q = 0$  the magnetic field is fully randomly ordered.

The poloidal magnetic field  $B_z$  produces a torque  $T_{\text{mag}}$  on a disc annulus, width  $\Delta R$ , of size (Livio & Pringle 1992)

$$T_{\text{mag}} = -4\pi R^2 \left( \frac{\langle B_z \rangle^2}{4\pi} \right) \Delta R. \quad (61)$$

Considering the change of angular momentum in the disc annulus, this can be combined to give

$$2\pi R \Delta R \frac{\partial}{\partial t} (\Sigma R^2 \Omega_K) + \Delta (2\pi R \Sigma v_R R^2 \Omega_K) = \Delta G + T_{\text{mag}}, \quad (62)$$

where the terms on the LHS describe the local change of angular momentum and the radial advection of angular momentum from neighbouring annuli, while the terms on the RHS describe the viscous and magnetic torques. Note that while angular momentum transport due to radial advection and the viscous torque for the whole disc reduce to the values at the inner and outer boundary,

the magnetic torque produces a local angular momentum loss term across the disc.

Given this additional term ( $T_{\text{mag}}$ ) in the angular momentum, equation (3) now becomes

$$\frac{\partial}{\partial t} (\Sigma R^2 \Omega_K) + \frac{1}{R} \frac{\partial}{\partial R} (R \Sigma v_R R^2 \Omega_K) = \frac{1}{2\pi R} \frac{\partial G}{\partial R} - 2R \left( \frac{\langle B_z \rangle^2}{4\pi} \right). \quad (63)$$

In contrast to King et al. (2004), we now take explicit account of the fact that the wind/jet, which removes angular momentum from the disc, may also remove a significant amount of mass. We assume that the magnetic outflow at radius  $R$  co-rotates with the disc along each field line, out to some Alfvén radius  $R_A (> R)$ . Then the local mass loss rate,  $L_\Sigma$ , is related to the torque by

$$2\pi R \Delta R L_\Sigma R_A^2 \Omega_K = T_{\text{mag}}, \quad (64)$$

which implies that

$$L_\Sigma = -\frac{2(R/R_A)^2}{\Omega_K R} \left( \frac{\langle B_z \rangle^2}{4\pi} \right). \quad (65)$$

The loss term leads to a modification of the continuity equation (2) in the form

$$\frac{\partial \Sigma}{\partial t} + \frac{1}{R} \frac{\partial}{\partial R} (R \Sigma v_R) = L_\Sigma. \quad (66)$$

Eqns. 66 and 63 now can be combined using the functional form of the viscous torque (eq. 4) to give

$$\begin{aligned} \frac{\partial \Sigma}{\partial t} &= \frac{3}{R} \frac{\partial}{\partial R} \left( \sqrt{R} \frac{\partial}{\partial R} (v_\Sigma \sqrt{R}) \right) \\ &+ \frac{4}{R} \frac{\partial}{\partial R} \left( \left( \frac{\langle B_z \rangle^2}{4\pi} \right) \sqrt{\frac{R^5}{GM}} \left( 1 - \left( \frac{R}{R_A} \right)^2 \right) \right) \\ &- 2 \left( \frac{\langle B_z \rangle^2}{4\pi} \right) \left( \frac{R}{R_A} \right)^2 \sqrt{\frac{R}{GM}}. \end{aligned} \quad (67)$$

For  $R = R_A$  the enhancement of angular momentum due to the extra torque  $T_{\text{mag}}$  is balanced by the loss of angular momentum taken away by the wind since it is taken away with the same lever arm (see eq. 64) and the poloidal magnetic field influences the evolution only through the mass loss. Note that King et al. (2004) essentially assumed that  $R_A = \infty$ , and thus that mass loss is not important in the model presented there. However we retain the ratio  $R_A/R$  as a parameter and allow for mass loss, since analytical estimates (Pudritz & Norman 1986) give  $R_A/R = 10$  while numerical simulations (Ouyed & Pudritz 1997) suggest  $R_A/R \approx 1.5$ . Unless otherwise stated we choose  $R_A/R = 3$  as the fiducial value.

The mass lost also removes the internal energy of the gas at a rate

$$Q_w = L_\Sigma U \approx L_\Sigma c_s^2, \quad (68)$$

and thus we also require a revised energy equation (see eq. 11) which is in the form

$$\begin{aligned} \frac{dq}{dt} &= \dot{e} + v_R \frac{\partial e}{\partial R} + 2\pi R \Delta R P \dot{H} + P \frac{\partial (2\pi R H v_R)}{\partial R} \\ &= 2\pi R \Delta R (Q^+ + Q_w - Q^-). \end{aligned} \quad (69)$$

We now have three equations (eqns. 67, 49 and 69) describing the evolution of the disc. These are integrated in time using a one-step Euler scheme. Advection is treated in a first-order, up-wind donor cell procedure. We note that the main observational output from the disc is the radiation  $L_{\text{rad}}$  coming from the disc (see eq. 42).

## 6.5 Magnetic diffusivity

Following King et al. (2004), we take the effective magnetic diffusivity  $\eta^*$  in eq. 49 to be

$$\eta^* = v_t \max(1, QR/H), \quad (70)$$

where we assume that the Prandtl number is of the order unity ( $\eta = v_t$ ), but allow it to be enhanced by a factor  $R/H$  (van Ballegooyen 1989; Lubow et al. 1994) and include large scale effects by multiplying it by the coherency factor  $Q$ . For further discussion see King et al. (2004).

## 6.6 The interplay between the timescales for the flickering

In this section we quantify the timescale argument for the appearance of flickering. As mentioned previously, fluctuations propagate through the disc, if the viscous timescale is shorter than the magnetic timescale, i.e. the timescale where we expect sufficient alignment of the poloidal magnetic field in neighbouring cells.

The viscous timescale is given by (Pringle 1981)

$$\tau_{\text{visc}} = \frac{1}{\alpha (H/R)^2} \tau_{\text{dyn}}, \quad (71)$$

where  $\tau_{\text{dyn}} = 1/\Omega_K$  stands for the dynamical timescale.  $H/R$  is the opening angle of the disc. The magnetic timescale, i.e. the timescale, on which we expect neighbouring field lines to be sufficiently aligned, is given by (Livio et al. 2003)

$$\tau_{\text{mag}} = 2^{R/H} k_d \tau_{\text{dyn}}. \quad (72)$$

Thus the condition for propagation is

$$r_\tau = \tau_{\text{mag}}/\tau_{\text{visc}} \geq 1, \quad (73)$$

which translates into

$$r_\tau = 2^{R/H} k_d \alpha (H/R)^2 \geq 1. \quad (74)$$

We plot the ratio  $r_\tau$  in Fig. 9 for different values of  $\alpha$ . The value of  $k_d$  is fixed to 10 (see Sect. 6.3). The ratio is smallest for  $(H/R)_{\text{min}} \approx 0.35$ . For  $\alpha = 0.1$  fluctuations formally propagate only for  $H/R \geq 0.5$  or  $H/R \leq 0.25$  only, while for  $\alpha = 1$  fluctuations can propagate for all  $H/R$ . In contrast to that, for  $\alpha = 0.01$  fluctuations only propagate for  $H/R \leq 0.1$ .

This is in line with findings of Churazov et al. (2001) who state that fluctuations close to the dynamical timescale are effectively damped in geometrically thin discs but can survive in geometrically thick discs since then the fluctuation timescale becomes comparable to the viscous timescale. In our model fluctuations formally survive for lower  $H/R$  ratios as well. Then, however, the magnetic timescale is so long that alignment becomes extremely rare. From the above analysis this probably puts a lower limit on the viscosity parameter  $\alpha$  of  $\alpha \geq 0.1$  since most of the variability is expected to come from a optically thin, but geometrically thick disc.

## 7 OBSERVATIONS OF THE FLICKERING IN THE THERMAL COMPONENT OF THE X-RAY SPECTRUM

Before describing the numerical simulations we first consider the likely observational scenario to which they are relevant. In generalising the work of King et al. (2004) to more physically realistic discs, we have initially confined ourselves to considering the standard accretion disc configuration, with the addition of heat advection. In general this is assumed to correspond in X-ray binaries to

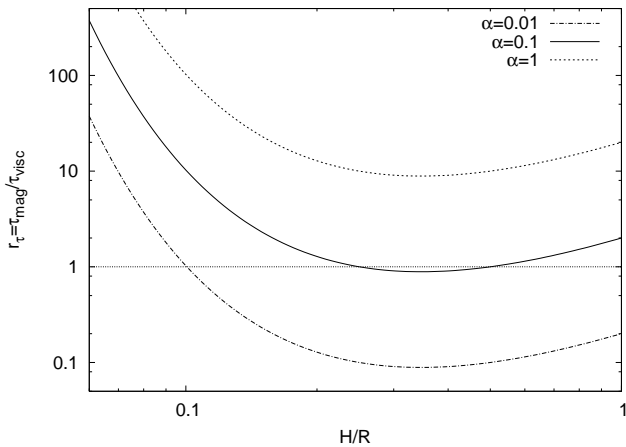


**Figure 9.** Ratio  $r_\tau$  of the magnetic and viscous timescale in dependence of  $H/R$  (see eq. 74) for different values of the viscosity parameter  $\alpha$  and  $k_d = 10$ . Only for  $r_\tau \geq 1$  fluctuations can propagate.

the thermally dominant (TD) or high/soft state. However, from an observational point of view, the variability in the TD or high/soft state is much less than in the LH state.

Usually the main components in the spectrum of X-Ray binaries can be well fit by a black-body and a power-law component (cf. McClintock & Remillard (2004)). The black-body or thermal component for galactic X-Ray binaries appears at energies around 1 keV, while the power-law component extends to higher energies. The components are thought to represent the radiation from the optically thick disc and a optically thin corona, respectively. Thus, since in the current paper, we only attempt to describe the time-dependent behaviour of the thermal disc component, i.e. the optically thick disc, we need to restrict ourselves to observations which explicitly concentrate on measuring the flickering in the thermal disc component of the X-Ray spectrum.

Churazov et al. (2001) show a power spectrum density (PSD) of Cyg X-1 in the high-soft state for energies of 6-13 keV, and state, that the amplitude in the softer bands is much smaller due to the influence of the black-body emission from the disc. They argue that their data is consistent with essentially all of the variability being associated with a power-law component and not with black-body emission (i.e. disc component), but do not quote a formal limit.

Miyamoto et al. (1994) examine Ginga observations of Nova Mus 1991 (GS 1124-683). They disentangle the variability in the disc and power-law component by calculating the PSD for different observations which have different fractional contributions from the power-law component to the total flux. For a power-law component fraction above approximately 10 per cent, the PSD at 0.3 Hz is an increasing function of power law fraction. While for lower values it is roughly constant ( $1.5 \cdot 10^{-5} \text{ Hz}^{-1}$ ). At these low values, the slope of the PSD is about -0.7 but due to the error bars it still could be fit with -0.5. Nowak et al. (1999) show that for counting noise dominated time-series the expected PSD slope is -0.5. Thus we conclude the data are consistent with a non-detection of flickering in the disc component. By using the value of the PSD at 0.3 Hz only we estimate an upper limit to the rms variability of  $r < 0.2$  per cent.

Nowak et al. (2001) consider LMC X-1 and LMC X-3. These are persistent black hole sources (i.e. not transients), and generally show spectra dominated by a soft, thermal component. They detect

no variability in LMC X-3 down to a level of about 0.8 per cent. They do detect variability in LMC X-1 of 7 per cent throughout the spectral range considered (0-9 keV), but since for LMC X-1 the power law component is much stronger than in LMC X-3, this could just be variability of the power law component.

Observations of the transient 4U 1543-47 during its 2002 outburst are presented in (Park et al. 2004). During most of the decay the spectrum is soft and dominated by black body emission. The PDS shape in this phase is roughly  $1/\nu$  and the variability is about  $r = 1$  per cent. However the fraction of black body emission never exceeds 80 per cent, i.e. the power law always contributes more than 20 per cent. Comparison with the results of Miyamoto et al. (1994) shows, that for a black-body flux fraction of 20 per cent, if the relation shown there is representative, the fractional rms must be  $r = 1$  per cent.

Kalemci et al. (2004) report on the light curves of a number of transients observed with RXTE. They again find strong variability in the low/hard state, while in the high/soft state they only can give upper limits, since they are counting noise dominated. Depending on the source, and the quality of the data, these limits are in the range 1 to 8 per cent.

To quantify the relation between the flux fraction and the rms variability, we have taken data from Kalemci et al. (2004) and Miyamoto et al. (1994) and plot the rms versus the black body flux fraction in Fig. 10. The fluxes are calculated in the 3-25 keV band. Since Miyamoto et al. (1994) only give the normalised power density  $P(\nu)$  at frequency  $\nu = 0.3$  Hz, we estimate the integrated rms  $r$  by using  $r = 2 \sqrt{\nu P_\nu}$ . The factor 2 is introduced to account for the  $d\nu/\nu$  in the definition of the integrated rms (cf. eq. 47). The black-body fraction for the LMC X-1 and X-3 data of Nowak et al. (2001) has been calculated using their black-body + powerlaw fits. While there is some scatter in the data, the global trend is that for black-body flux fractions lower than 5 per cent the rms variability is about 25 per cent, while it drops beyond detectable limits for larger values of the black body fraction. The transition is not very sharp, but occurs around a black body fraction in the range 3 to 20 per cent. The transition might be sharper than this but we are only using data in the 3-25 keV range where the black-body contribution is small compared to the power-law component, and varies from source to source. In addition, we note that Zdziarski et al. (2005) carry out an energy-dependent analysis of the fractional rms for GRS 1915+105 and come to similar conclusions.

To summarise, it is clear from the observations that the rms variability of the black-body component in the X-Ray spectra of black hole sources is small. Indeed there are no clear detections, but only upper limits. As a representative value we take  $r = 1$  per cent as an upper limit for the variability of the thermal component.

## 8 RESULTS

To demonstrate the effect of the stochastic magnetic wind/jet on our disc models model with the physical input so far, we ran some models to assess the influence of the parameters on the variability. For all models, we fix the mass of the black hole to be  $10 M_\odot$ , the viscosity parameter  $\alpha = 0.1$  (appropriate for standard optically thick discs, see Lewin et al. 1997) and take for the dynamo timescale (cf. eq. 50)  $k_d = 10$ .

First we consider a black hole accreting at half of the Eddington rate,  $\dot{M} = 0.5 \dot{M}_{\text{Edd}}$ . We take the Alfvén radius at each radius to be a constant value of  $R_A/R = 3$ . From Figure 4, in the absence of magnetic flickering (i.e. with  $\beta_S = 0$ ) the disc is unstable and

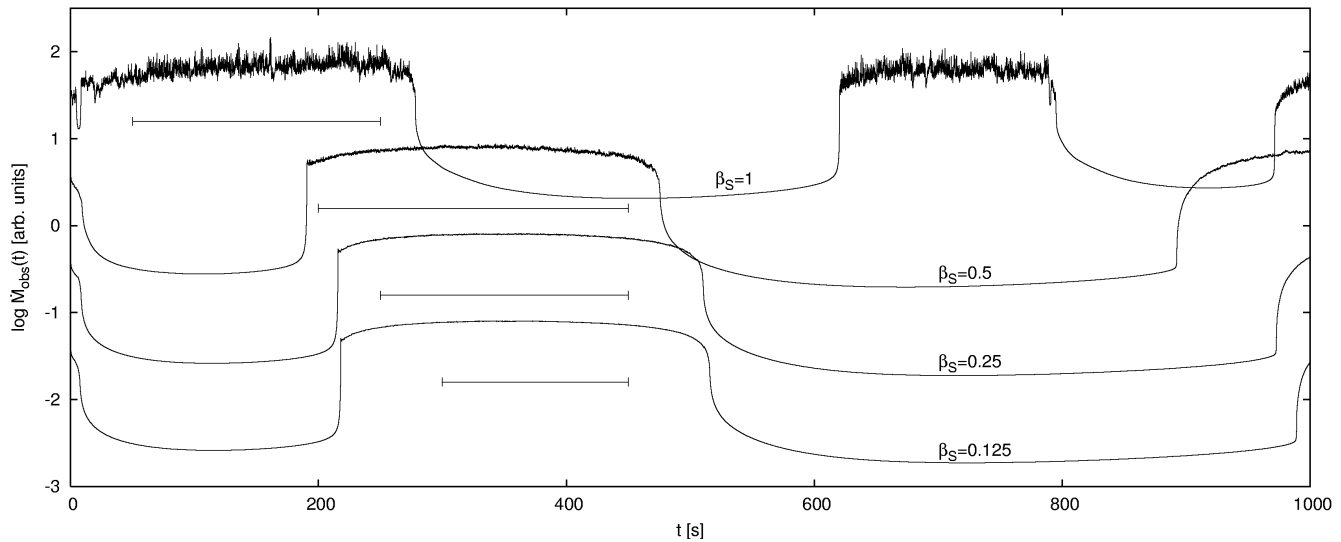


**Figure 11.** Sample lightcurves for a  $10 M_{\odot}$  mass black hole accreting at  $0.5 \dot{M}_{\text{Edd}}$  for different values of  $\beta_S$ , the strength of the poloidal field compared to the disc magnetic field. The ratio of the Alfvén radius  $R_A$  to the radial distance  $R$  is  $R_A/R = 3$ , the viscosity parameter  $\alpha = 0.1$ . The intervals indicate the time-segments shown in Fig. 12 used to calculate the power spectra shown in Fig. 13.

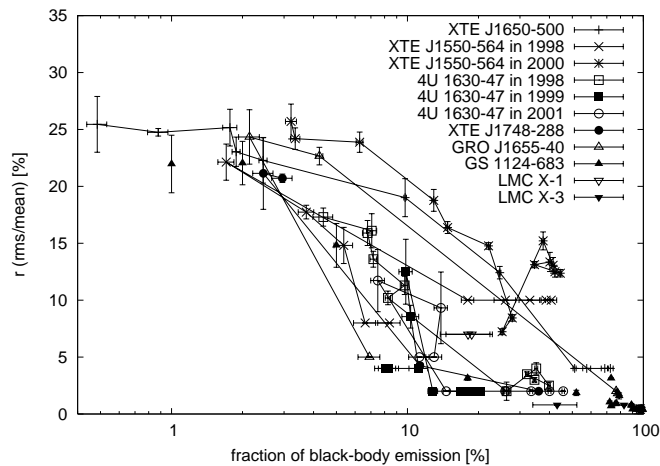


**Figure 10.** Fractional rms variability  $r$  for different black-body flux fractions in the 3-25 keV band for different objects. All data from Kalemci et al. (2004) except the data for GS 1124-683, which have been taken from Miyamoto et al. (1994) and LMC X-1 and X-3 from Nowak et al. (2001).

shows limit-cycle behaviour. Fig. 11 shows sample lightcurves for different values of  $\beta_S$ . The limit cycle is still present, i.e. the disc oscillates between a high  $\dot{M}_{\text{obs}}$  and low  $\dot{M}_{\text{obs}}$  state. It is best evident from the  $\beta_S = 1$  case that while in the high  $\dot{M}_{\text{obs}}$  state there is some variability, in the low  $\dot{M}_{\text{obs}}$  state there is hardly any sign of variability. This is a result of the smaller  $H/R$  ratio in the inner disc during the low  $\dot{M}_{\text{obs}}$  state. Then the alignment timescale (proportional to the factor  $2^{R/H}$  times the dynamical timescale, see Livio et al. 2003) is much longer than the viscous timescale (proportional to  $(R/H)^2$  times the dynamical timescale): Fluctuations formally could survive, but since alignment occurs on extremely long timescales only, they are unlikely to produce flickering (see Section 6.6 and King et al. 2004). In the high- $\dot{M}$  state, however, both timescales are at least comparable and so fluctuations propagate to the inner disc without being smeared out by the viscosity.

It is evident from Fig. 11, that a non-zero  $\beta_S$  influences the

strength of the variability. In Fig. 13 we show the influence of the parameter  $\beta_S$  on the power density spectra (PDS), while the integrated fractional rms  $r$  (see eq. 47) is shown in Fig. 14.

The time segments used for the calculation of the PDS are indicated in Fig. 11. Throughout this section, we only take segments from the lightcurve, where the disc was in the high- $\dot{M}$  state. Since for red-noise the lightcurve is only a stochastic realisation of the underlying process, the calculated PDS fluctuates randomly around the “true” spectrum (e.g. Uttley et al. 2002). To overcome this difficulty, we divided each segment in 10 equally spaced sub-segments, calculated the PDS of each subsegment and took the average of these. We further normalised each subsegment to remove linear trends in the lightcurve.

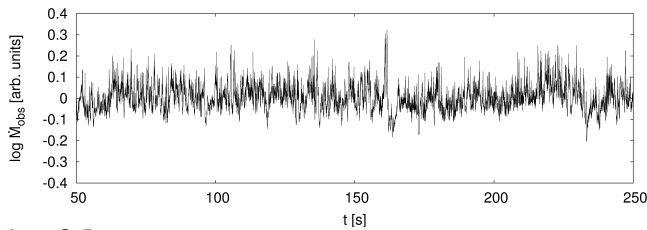
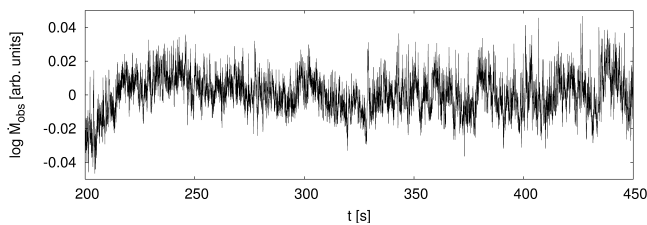
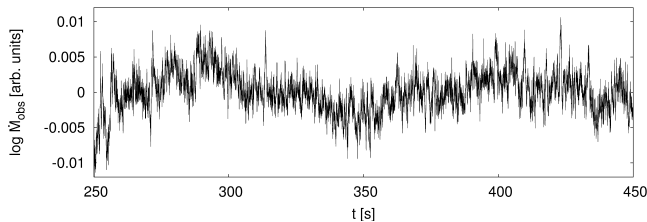
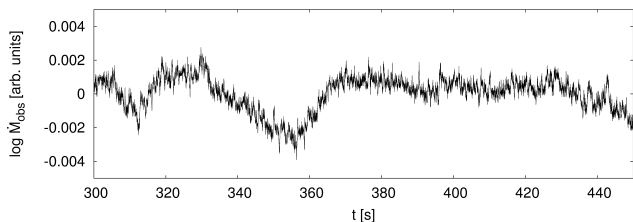
We see from Fig. 14 that the rms variability is  $r < 1\%$ , for  $\beta_S < 0.2$  and that  $r$  strongly increases for larger  $\beta_S$  and reaching 10-20 % for  $\beta_S = 1$ . The near quadratic increase of  $r$  with  $\beta_S$  reflects the fact, that the poloidal magnetic field influences the disc only through the torque which is proportional to  $\langle B_z^2 \rangle$  which in turn is proportional to  $\beta_S^2 P$ , i.e. a fraction  $\beta_S^2$  of the viscous torque (see eqns. 61, 52, 51 and 22).

Given the observational constraints, discussed in Section 7, it is evident that we need to take  $\beta_S$  to be smaller than around 0.1 - 0.2. Thus in this model we require the energy density in the poloidal field component to be at most only a few percent of the energy density in the magnetic field generated by MRI in the disc.

Next we consider the influence of the accretion rate on the variability for constant  $\beta_S$ . Fig. 15 shows the PDS for two values of  $\beta_S$  for different accretion rates. While the integrated rms variability  $r$  does not depend on the accretion rate but on  $\alpha$ , the shape of the PDS for different accretion rates is slightly different.

We also briefly investigate the behaviour which occurs if  $\beta_S$ , the ratio of poloidal and tangled magnetic field strengths, is assumed to vary with  $H/R$ . For example, in their simple dynamo model, Tout & Pringle (1996) suggest that  $\beta_S$  might be proportional to  $H/R$ . If so, since  $H/R$  in the simulations described is at most  $H/R \sim 1/5$ , we can put a constraint on the constant of proportionality to be smaller than unity.

In Figures 16 and 17 we show the results of simulations with

$\beta_S = 1$  $\beta_S = 0.5$  $\beta_S = 0.25$  $\beta_S = 0.125$ 

**Figure 12.** Lightcurve segments for the cases shown in Fig. 11 for different  $\beta_S$ . These are used to calculate the PDS in Fig. 13.  $M_{\text{obs}}$  is given in arbitrary units, but the amplitude still has got some meaning. Note that the overall shape of the lightcurve does not change considerably, while the range in  $M_{\text{obs}}$  changes significantly. The longterm trend in the data has been removed.

the same parameters as before but with  $\beta_S = 0.5H/R$  and  $\beta_S = H/R$  for varying accretion rate. For the  $1 \dot{M}_{\text{Edd}}$  cases there is a significant decline of the PDS for small frequencies. This decline is a result of a declining  $H/R$  in the outer disc which shortens the amplitude of flares released from further out (i.e. longer timescales) through the  $H/R$ -dependence of  $\beta_S$ . For the lower accretion rates this decline is far less obvious, but then the time the disc is spending in the high- $\dot{M}$  state is becoming shorter and so does the time available for the FFT and averaging. The integrated fractional rms in for the same accretion rate changes by a factor of about 4 when comparing the cases of  $\beta_S = 0.5H/R$  and  $\beta_S = H/R$  consistent with the result of Fig. 14 where we show the quadratic dependence of  $r$  with  $\beta_S$ .

Finally we explored the influence of different values of  $R_A/R$  on the variability. In Figure 18 we show the influence for a  $10 M_{\odot}$  black hole accreting at  $0.5 \dot{M}_{\text{Edd}}$  with  $\beta_S = 0.25$ . The system changes with  $R_A/R$  increasing from a mass loss to a mag-

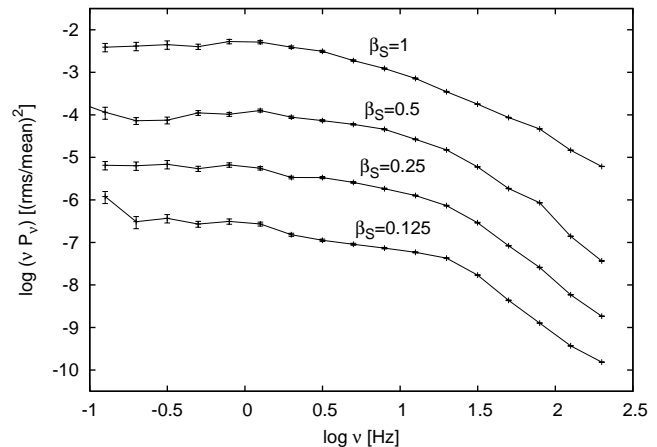


**Figure 13.** Power spectra for a  $10 M_{\odot}$  model solar mass black hole, accreting at  $0.5 \dot{M}_{\text{Edd}}$  for different values of  $\beta_S$  for the lightcurve segments shown in Fig. 12.  $\alpha = 0.1$

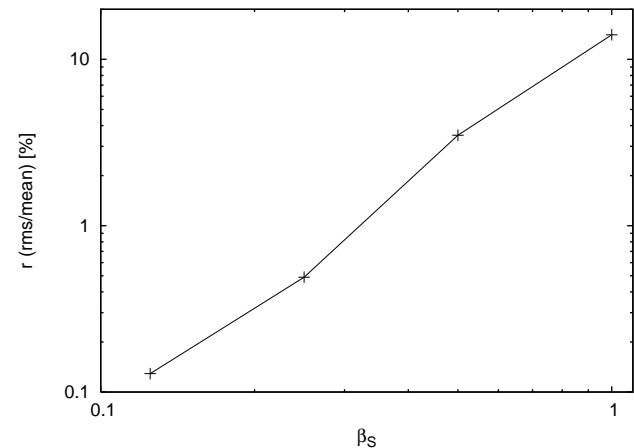


**Figure 14.** Integrated fractional rms  $r$  for a  $10 M_{\odot}$  model solar mass black hole, accreting at  $0.5 \dot{M}_{\text{Edd}}$  in dependence of  $\beta_S$ , the strength of the poloidal field compared to the disc magnetic field (cf. Fig. 13). The viscosity parameter is  $\alpha = 0.1$ .

netic torque dominated regime. For the parameters chosen, the integrated rms-variability  $r$  is increasing with  $R_A/R$  and saturates for  $R_A/R > 3$ . The power spectral shape then is indistinguishable within the error bars. Thus the assumption of King et al. (2004) who set  $R_A/R = \infty$  is justified as long as the "real"  $R_A/R > 3$ .

## 9 CONCLUSIONS

We have generalised the model of King et al. (2004) for variability in black hole accretion discs by including proper consideration of the local disc structure. We take the disc properties to depend only on radius  $R$ , and so, in common with other authors, make a local one-zone approximation for the disc structure.

In the absence of the addition of a stochastic magnetic dynamo, which drives the flickering, we mainly reproduce results similar theoretical work has shown. We agree that taking account

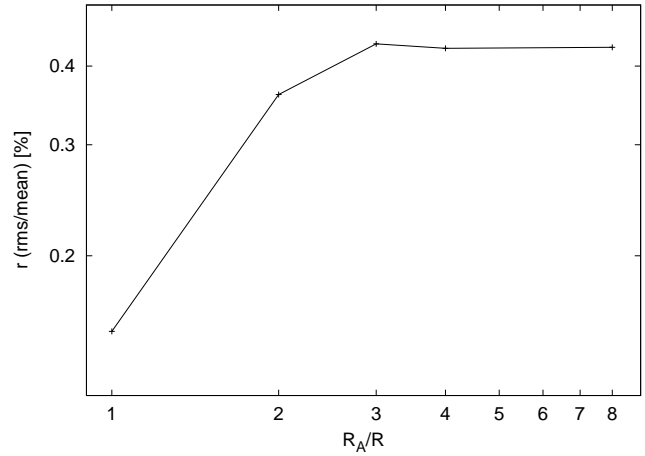
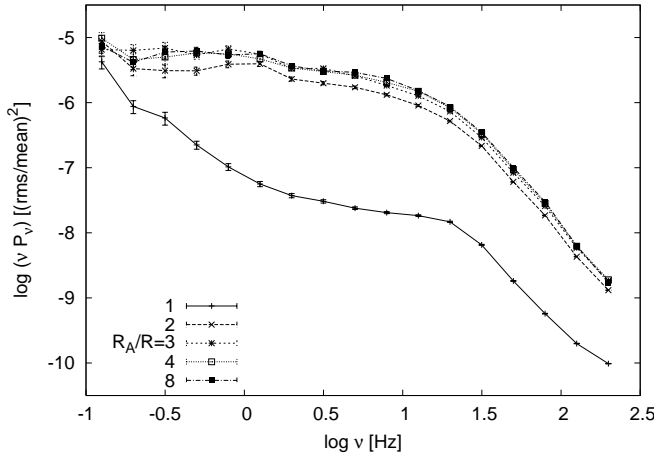


**Figure 18.** (left) Power spectra for different values of  $R_A/R$ , the ratio of the Alfvén radius  $R_A$  to the radial distance  $R$  for a  $10 M_\odot$  black hole accreting at  $0.5 \dot{M}_{\text{Edd}}$  with  $\beta_S = 0.25$ , the ratio of the poloidal field compared to the disc magnetic field. (right) Integrated rms-variability  $r$  as a function of  $R_A/R$ . For all  $R_A/R > 3$  the power spectra and the value of  $r$  is essentially indistinguishable.

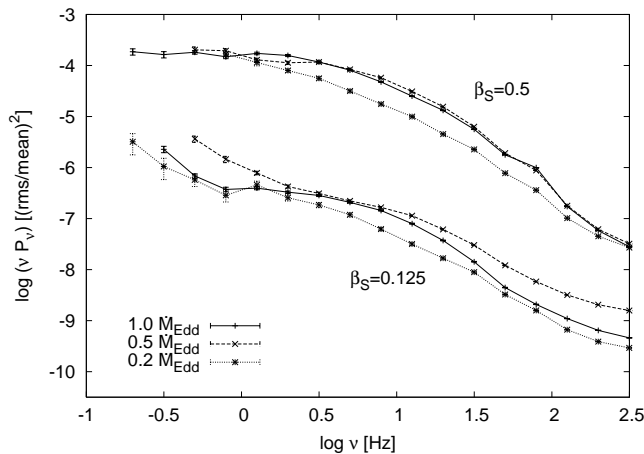


**Figure 15.** Power spectra for a  $10 M_\odot$  model solar mass black hole, accreting at different accretion rates for different  $\beta_S = 0.125$  and  $0.5$ .  $\alpha = 0.1$ .

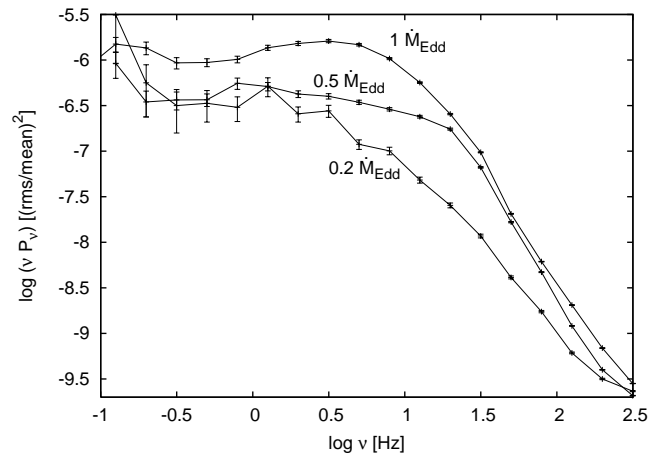


**Figure 16.** Power spectra for a  $10 M_\odot$  model solar mass black hole, accreting at different rates for  $\beta_S = 0.5$  ( $H/R$ ).  $\alpha = 0.1$ .

to advective heat flow is of crucial importance in determining the structure of the inner regions, but find that the assumption of strictly Keplerian angular velocities, and the neglect of radial pressure gradients, are generally reasonable assumptions.

When a stochastic dynamo is included we find behaviour similar to that described by King et al. (2004). However, because the degree of variability of the thermal disc is observed to be small (less than around 1 per cent), if it is detected at all, we can only draw limited conclusions. Our main finding is that for consistency we require that the strength of the poloidal field generated by any radial disc dynamo cell must be at least an order of magnitude smaller than the field generated by the dynamo within the disc. The simulations reported here however are of help to understand the influence of the parameters on the variability.

In this paper we have restricted ourselves to modelling just the thermal disc component, and so have had to restrict our attention to the high/soft or thermally dominant state of black hole binaries. In future work we shall begin to include consideration of a hot corona, in addition to the cooler thermal disc, so that we can begin to model

the more highly variable low/soft state of the black hole binaries, as well as the X-rays from AGN (Uttley et al. 2005).

## ACKNOWLEDGEMENTS

MM gratefully acknowledges financial support from PPARC. We also thank the anonymous referee for comments on the paper which helped to improve it significantly.

## REFERENCES

- Abe Y., Fukazawa Y., Kubota A., Kasama D., Makishima K., , 2005, Three Spectral States of the Disk X-Ray Emission of the Black-Hole Candidate 4U 1630-47
- Abramowicz M. A., Czerny B., Lasota J. P., Szuszkiewicz E., 1988, ApJ, 332, 646
- Belloni T., Hasinger G., 1990, A&A, 230, 103

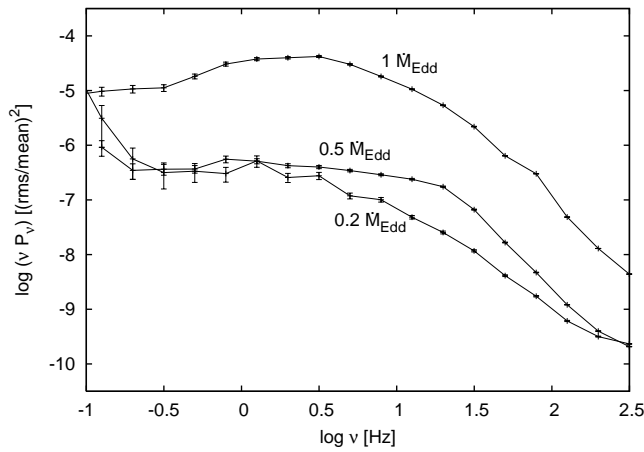


**Figure 17.** Power spectra for a  $10 M_{\odot}$  model solar mass black hole, accreting at different rates for  $\beta_S = (H/R)$ .  $\alpha = 0.1$ .

Bisnovaty-Kogan G. S., Lovelace R. V. E., 2001, *New Astronomy Review*, 45, 663  
 Churazov E., Gilfanov M., Revnivtsev M., 2001, *MNRAS*, 321, 759  
 Clarke C. J., 1988, *MNRAS*, 235, 881  
 Clarke C. J., Shields G. A., 1989, *ApJ*, 338, 32  
 Faulkner J., Lin D. N. C., Papaloizou J., 1983, *MNRAS*, 205, 359  
 Frank J., King A., Raine D. J., 2002, *Accretion Power in Astrophysics: Third Edition*. *Accretion Power in Astrophysics*, by Juhan Frank and Andrew King and Derek Raine, pp. 398. ISBN 0521620538. Cambridge, UK: Cambridge University Press, February 2002.  
 Grevesse N., Noels A., 1993, in Pratzto M., Vangioni-Flam E., Casse M., eds, *Origin and Evolution of the Elements Solar composition*. Cambridge University Press, p. 15  
 Hameury J., Menou K., Dubus G., Lasota J., Hure J., 1998, *MNRAS*, 298, 1048  
 Honma F., Kato S., Matsumoto R., 1991, *PASJ*, 43, 147  
 Iglesias C. A., Rogers F. J., 1996, *ApJ*, 464, 943  
 Janiuk A., Czerny B., Siemiginowska A., 2002, *ApJ*, 576, 908  
 Kalemci E., Tomsick J. A., Rothschild R. E., Pottschmidt K., Kaaret P., 2004, *ApJ*, 603, 231  
 King A. R., Pringle J. E., West R. G., Livio M., 2004, *MNRAS*, 348, 111  
 Kiriakidis M., El Eid M. F., Glatzel W., 1992, *MNRAS*, 255, 1P  
 Kubota A., Makishima K., 2004, *ApJ*, 601, 428  
 Lasota J.-P., 2001, *New Astronomy Review*, 45, 449  
 Lewin W. H. G., van Paradijs J., van den Heuvel E. P. J., 1997, *X-ray Binaries*. *X-ray Binaries*, Edited by Walter H. G. Lewin and Jan van Paradijs and Edward P. J. van den Heuvel, pp. 674. ISBN 0521599342. Cambridge, UK: Cambridge University Press, January 1997.  
 Lewin W. H. G., van Paradijs J., van der Klis M., 1988, *Space Science Reviews*, 46, 273  
 Lightman A. P., Eardley D. M., 1974, *ApJ*, 187, L1  
 Livio M., Pringle J. E., 1992, *MNRAS*, 259, 23P  
 Livio M., Pringle J. E., King A. R., 2003, *ApJ*, 593, 184  
 Lubow S. H., Papaloizou J. C. B., Pringle J. E., 1994, *MNRAS*, 267, 235  
 Lyubarskii Y. E., 1997, *MNRAS*, 292, 679

Markowitz A., Edelson R., Vaughan S., Uttley P., George I. M., Griffiths R. E., Kaspi S., Lawrence A., McHardy I., Nandra K., Pounds K., Reeves J., Schurch N., Warwick R., 2003, *ApJ*, 593, 96  
 Mayer M., Duschl W. J., 2005, *MNRAS*, 356, 1  
 McClintock J., Remillard R., 2004, in Lewin W., van der Klis M., eds, *Compact Stellar X-ray Sources Black hole binaries*. Cambridge University Press  
 McHardy I., 1988, *Memorie della Societa Astronomica Italiana*, 59, 239  
 Miyamoto S., Kitamoto S., Iga S., Hayashida K., Terada K., 1994, *ApJ*, 435, 398  
 Muchotrzeb B., Paczynski B., 1982, *Acta Astronomica*, 32, 1  
 Nayakshin S., Rappaport S., Melia F., 2000, *ApJ*, 535, 798  
 Nowak M. A., Vaughan B. A., Wilms J., Dove J. B., Begelman M. C., 1999, *ApJ*, 510, 874  
 Nowak M. A., Wilms J., Heindl W. A., Pottschmidt K., Dove J. B., Begelman M. C., 2001, *MNRAS*, 320, 316  
 Ouyed R., Pudritz R. E., 1997, *ApJ*, 482, 712  
 Park S. Q., Miller J. M., McClintock J. E., Remillard R. A., Orosz J. A., Shrader C. R., Hunstead R. W., Campbell-Wilson D., Ishwara-Chandra C. H., Rao A. P., Rupen M. P., 2004, *ApJ*, 610, 378  
 Pringle J. E., 1976, *MNRAS*, 177, 65  
 Pringle J. E., 1981, *ARA&A*, 19, 137  
 Pringle J. E., Verbunt F., Wade R. A., 1986, *MNRAS*, 221, 169  
 Pudritz R. E., Norman C. A., 1986, *ApJ*, 301, 571  
 Rogers F. J., Iglesias C. A., 1992, *ApJ*, 401, 361  
 Seaton M. J., Yan Y., Mihalas D., Pradhan A. K., 1994, *MNRAS*, 266, 805  
 Shakura N. I., Sunyaev R. A., 1973, *A&A*, 24, 337  
 Simon N. R., 1982, *ApJ*, 260, L87  
 Stone J. M., Hawley J. F., Gammie C. F., Balbus S. A., 1996, *ApJ*, 463, 656  
 Szuszkiewicz E., Miller J. C., 1997, *MNRAS*, 287, 165  
 Szuszkiewicz E., Miller J. C., 1998, *MNRAS*, 298, 888  
 Szuszkiewicz E., Miller J. C., 2001, *MNRAS*, 328, 36  
 Tout C. A., Pringle J. E., 1992, *MNRAS*, 259, 604  
 Tout C. A., Pringle J. E., 1996, *MNRAS*, 281, 219  
 Uttley P., 2004, *MNRAS*, 347, L61  
 Uttley P., McHardy I. M., 2001, *MNRAS*, 323, L26  
 Uttley P., McHardy I. M., Papadakis I. E., 2002, *MNRAS*, 332, 231  
 Uttley P., McHardy I. M., Vaughan S., 2005, *MNRAS*, 359, 345  
 van Ballegooijen A. A., 1989, in *ASSL Vol. 156: Accretion Disks and Magnetic Fields in Astrophysics Magnetic fields in the accretion disks of cataclysmic variables*. pp 99–106  
 van der Klis M., 1994, *ApJS*, 92, 511  
 Vaughan S., Edelson R., Warwick R. S., Uttley P., 2003, *MNRAS*, 345, 1271  
 Zdziarski A. A., Gierliński M., Rao A. R., Vadawale S. V., Mikołajewska J., 2005, *MNRAS*, 360, 825

## APPENDIX A: THE ENERGY EQUATION

### A1 Derivation of the LHS

The first law of thermodynamics is

$$dQ = dE + Pd\left(\frac{1}{\rho}\right), \quad (\text{A1})$$



where  $dQ$  stands for the change in heat  $Q$  per unit mass,  $dE$  the change in internal energy  $E$  per unit mass, and  $Pd(1/\rho)$  the volume work.  $P$  is the pressure and the specific volume is  $1/\rho$ .

The continuity equation in general form reads

$$d(\rho V) = \rho dV + V d\rho = 0, \quad (\text{A2})$$

which is equivalent to

$$\frac{dV}{V} = -\frac{d\rho}{\rho}. \quad (\text{A3})$$

In total differentials using the continuity equation, the energy equation can be shown to be equivalent to

$$d(\rho V Q) = d(\rho V E) + P dV. \quad (\text{A4})$$

This relation implies that the change of total heat in a volume  $V$  is given by a change in the total internal energy and the expansion of the volume.

In cylindrical coordinates, vertically averaged, we have

$$V = 2\pi R H \Delta R \quad (\text{A5})$$

Thus

$$d(\pi R \Sigma \Delta R Q) = d(\pi R \Sigma \Delta R E) + 2\pi R \Delta R P dH. \quad (\text{A6})$$

Replacing the specific heat  $Q$  by the total heat content  $q$  in a semidisc annulus,

$$q = \pi R \Sigma \Delta R Q, \quad (\text{A7})$$

and the specific internal energy  $E$  by the total internal energy  $e$  in a semidisc annulus,

$$e = \pi R \Sigma \Delta R E, \quad (\text{A8})$$

we can write

$$dq = de + P d(2\pi R H \Delta R). \quad (\text{A9})$$

Time-dependently, the LHS of the energy equation is written

$$\frac{dq}{dt} = \frac{de}{dt} + P \frac{d(2\pi R H \Delta R)}{dt}. \quad (\text{A10})$$

Taking into account advection, with radial velocity  $u_R$ ,

$$\frac{dq}{dt} = \dot{e} + u_R \frac{\partial e}{\partial R} + 2\pi R \Delta R P \dot{H} + P \frac{\partial (2\pi R H u_R)}{\partial R}. \quad (\text{A11})$$

In discretized form,

$$\frac{dq}{dt} = \dot{e} + \Delta(\pi R u_R \Sigma E) + 2\pi R \Delta R P \dot{H} + P \Delta(2\pi R u_R H_{\text{ad}}), \quad (\text{A12})$$

where  $H_{\text{ad}}$  is the advected value of  $H$ , and this term corresponds to the advected volume contributing to the 'PdV' work.

Now, given the specific internal energy  $E$ , where

$$E = \frac{3}{2} \frac{kT}{\mu m_p} + \frac{4\sigma}{cp} T^4, \quad (\text{A13})$$

and given hydrostatic equilibrium in the form

$$\rho \frac{kT}{\mu m_p} + \frac{4\sigma}{3c} T^4 = G \frac{M}{4\rho R^3} \Sigma^2, \quad (\text{A14})$$

$\rho$  and  $T$  can now be computed, for given values of  $E$  and  $\Sigma$ . The variation of  $H$  in terms of  $E$  and  $\Sigma$  is given by using the definition of the surface density (Equation 1)

$$\frac{dH}{H} = \frac{d\Sigma}{\Sigma} - \frac{d\rho}{\rho}. \quad (\text{A15})$$

Using both the hydrostatic equilibrium, and the definition of the

internal energy  $E$ , we can express the variation in  $\rho$  in terms of variations in the surface density  $\Sigma$  and specific internal energy  $E$  as

$$\frac{d\rho}{\rho} = \frac{8 - 6\eta}{8 + \beta_p - 7\eta} \frac{d\Sigma}{\Sigma} - \frac{4 - 3\beta_p}{8 + \beta_p - 7\eta} \frac{dE}{E}. \quad (\text{A16})$$

With the combination of the last two equations we can eliminate  $d\rho/\rho$  to obtain

$$\frac{dH}{H} = \frac{\beta_p - \eta}{8 + \beta_p - 7\eta} \frac{d\Sigma}{\Sigma} + \frac{4 - 3\beta_p}{8 + \beta_p - 7\eta} \frac{dE}{E}, \quad (\text{A17})$$

$$= \frac{4\beta_p - 4 - \eta}{8 + \beta_p - 7\eta} \frac{d\Sigma}{\Sigma} + \frac{4 - 3\beta_p}{8 + \beta_p - 7\eta} \frac{de}{e}, \quad (\text{A18})$$

$$= \frac{4\beta_p^2 - 11\beta_p + 8}{\beta_p^2 + 13\beta_p - 16} \frac{d\Sigma}{\Sigma} + \frac{-3\beta_p^2 + 10\beta_p - 8}{\beta_p^2 + 13\beta_p - 16} \frac{de}{e}, \quad (\text{A19})$$

$$(\text{A20})$$

where we use

$$\eta = \frac{E_{\text{gas}}}{E}, \quad (\text{A21})$$

and

$$\beta_p = \frac{P_{\text{gas}}}{P}, \quad (\text{A22})$$

as the fractional contribution of the gas component to the specific internal energy and pressure, respectively. These two variables are related by

$$\eta = \frac{\beta_p}{2 - \beta_p}. \quad (\text{A23})$$

The specific internal energy and pressure are related by

$$E = \frac{P}{\rho} \left( 3 - \frac{3}{2} \beta_p \right). \quad (\text{A24})$$

Equation A19, multiplied by  $H$  and taking the time-derivative leads to (using Equations (A23) and (1))

$$\dot{H} = \underbrace{\frac{4\beta_p^2 - 11\beta_p + 8}{\beta_p^2 + 13\beta_p - 16}}_{C_\Sigma} \frac{\dot{\Sigma}}{2\rho} + \underbrace{\frac{-3\beta_p^2 + 10\beta_p - 8}{\beta_p^2 + 13\beta_p - 16}}_{C_e} \frac{\dot{e}}{2\pi R \rho \Delta R E} \quad (\text{A25})$$

The coefficients  $C_e$  and  $-C_\Sigma$  are equal to  $\frac{1}{2}$  for  $\beta_p \rightarrow 0$  and  $\beta_p \rightarrow 1$ , while going through a minimum for  $\beta_p \approx 0.75$  at values 0.38 and 0.35, respectively. Then in both the limiting cases of  $\beta_p \rightarrow 0$  and  $\beta_p \rightarrow 1$ , we find  $H \propto \sqrt{e/\Sigma} \approx \sqrt{\Sigma c_s^2/\Sigma} = c_s$ , recovering the hydrostatic equilibrium.

Using Equation (A25) in the energy equation (A12), we can write

$$\begin{aligned} \frac{dq}{dt} &= \dot{e} + \Delta(\pi R u_R \Sigma E) + 2\pi R \Delta R P \dot{H} + P \Delta(2\pi R u_R H_{\text{ad}}) \\ &= \dot{e} \left( 1 + C_e \frac{P}{\rho E} \right) + \Delta(\pi R u_R \Sigma E) + \pi R \Delta R \frac{P}{\rho} C_\Sigma \dot{\Sigma} + 2\pi R P \Delta(u_R H_{\text{ad}}) \\ &= \dot{e} \left( 1 + C_e \frac{P}{\rho E} \right) + \Delta \left( \frac{1}{2} \dot{M} E_{\text{ad}} \right) + \pi R \Delta R \frac{P}{\rho} C_\Sigma \dot{\Sigma} + \frac{1}{2} P \Delta \left( \dot{M} \frac{1}{\rho_{\text{ad}}} \right), \end{aligned}$$

where we applied  $\dot{M} = 2\pi \Sigma R u_R$  in the last step.

## APPENDIX B: LOCAL STABILITY ANALYSIS

The thermal stability analysis (Pringle 1976), now including advection shows thermal instability for

$$\left( \frac{\partial \log Q^+}{\partial \log T} \right)_p - \left( \frac{\partial \log(Q^- + Q_{\text{ad}})}{\partial \log T} \right)_p > 0. \quad (\text{B1})$$

Thermal instability occurs, if the increase(decrease) of temperature compared to the equilibrium state leads to a stronger increase(decrease) of the heating compared to the cooling while keeping hydrostatic equilibrium.

Using the equilibrium condition ( $Q^+ = Q^- + Q_{\text{ad}}$ ) and

$$\epsilon_{\text{ad}} = \frac{Q_{\text{ad}}}{Q_{\text{ad}} + Q^-}, \quad (\text{B2})$$

we get the condition

$$\left( \frac{\partial \log Q^+}{\partial \log T} \right)_p - \epsilon \left( \frac{\partial \log Q_{\text{ad}}}{\partial \log T} \right)_p - (1 - \epsilon) \left( \frac{\partial \log Q^-}{\partial \log T} \right)_p > 0. \quad (\text{B3})$$

Along similar lines, viscous instability (e.g. Lightman & Eardley 1974; Pringle 1981) only occurs as long as

$$\left( \frac{\partial \log \dot{M}}{\partial \log \Sigma} \right)_{p,T} < 0. \quad (\text{B4})$$

The disc is viscously unstable, if an increase(decrease) of accretion rate does lead to a lower/higher surface density.

For the calculation of the criterion we use the hydrostatic equilibrium

$$\log P - \log \frac{GM}{4\rho R^3} \Sigma^2 = f_1(\rho, T, \Sigma) = 0, \quad (\text{B5})$$

and the stationary energy equation

$$\log Q^+ - \log(Q^- + Q_{\text{ad}}) = f_2(\rho, T, \Sigma) = 0. \quad (\text{B6})$$

With the contribution of gas and radiation to the total pressure (see eq. 16) we can write the total variation of the hydrostatic equilibrium and energy equation in terms of  $\rho$ ,  $T$  and  $\Sigma$ , generalising the method of Mayer & Duschl (2005) for a non selfgravitating, optically thick accretion disc. We neglect changes in  $\chi_{\text{ad}}$  since  $\chi_{\text{ad}}$  is expected to vary only very little.

We take the variation of the hydrostatic equilibrium ( $f_1$ )

$$A \frac{d\rho}{\rho} + B \frac{dT}{T} + C \frac{d\Sigma}{\Sigma} = 0 \quad (\text{B7})$$

and the stationary energy equation ( $f_2$ )

$$D \frac{d\rho}{\rho} + E \frac{dT}{T} + F \frac{d\Sigma}{\Sigma} = 0 \quad (\text{B8})$$

with respect to  $\rho$ ,  $T$  and  $\Sigma$ . The coefficients  $A \dots E$  are

$$A = \frac{\partial f_1}{\partial \log \rho} = 1 + \beta_p \quad (\text{B9})$$

$$B = \frac{\partial f_1}{\partial \log T} = 4 - 3\beta_p \quad (\text{B10})$$

$$C = \frac{\partial f_1}{\partial \log \Sigma} = -2 \quad (\text{B11})$$

$$D = \frac{\partial f_2}{\partial \log \rho} = A_{\text{R}}(1 - \epsilon_{\text{ad}}) + (\beta_p - 1)(1 - 2\epsilon_{\text{ad}}) \quad (\text{B12})$$

$$E = \frac{\partial f_2}{\partial \log T} = (B_{\text{R}} - 4)(1 - \epsilon_{\text{ad}}) + (4 - 3\beta_p)(1 - 2\epsilon_{\text{ad}}) \quad (\text{B13})$$

$$F = \frac{\partial f_2}{\partial \log \Sigma} = 2(1 - \epsilon_{\text{ad}}) \quad (\text{B14})$$

with

$$(A_{\text{R}}, B_{\text{R}}) = \frac{\partial \log \kappa_{\text{R}}}{\partial \log(\rho, T)}. \quad (\text{B15})$$

Thermal instability exists, if

$$AE - BD > 0 \quad (\text{B16})$$

where we used the variation of the energy equation and expressed the density variation  $d\rho/\rho$  in terms of temperature  $dT/T$  using the variation of the hydrostatic equilibrium while keeping the surface density  $\Sigma = \text{const}$ .

We have viscous instability for

$$-(\beta_p - 1) \frac{CE - BF}{AE - BD} - (4 - 3\beta_p) \frac{AF - CD}{AE - BD} + 1 < 0 \quad (\text{B17})$$

where we both expressed the density and temperature variations in terms of the surface density variations and use this expression in the angular momentum equation

$$\dot{M} - 3\pi\nu_1\Sigma = 0 \quad (\text{B18})$$

to get the instability criterion.

In the radiation pressure ( $\beta_p = 0$ ) and Thomson scattering ( $A_{\text{R}} = B_{\text{R}} = 0$ ) dominated regime we get thermal instability only if

$$4 - 12\epsilon_{\text{ad}} > 0 \quad (\text{B19})$$

and viscous instability as long as

$$\frac{7(\epsilon_{\text{ad}} - 1)}{1 - 3\epsilon_{\text{ad}}} < 0 \quad (\text{B20})$$

Since the nominator of the LHS of the last expression is always negative ( $0 < \epsilon_{\text{ad}} < 1$ ), the condition of thermal instability and viscous instability are the same.

To conclude, thermal and viscous instability only occurs, if  $\epsilon_{\text{ad}} < \frac{1}{3}$ . A radiation pressure dominated disc can be thermally and viscously unstable as long as advection only contributes less than one third of the local energy loss. This clearly shows the stabilising effect of energy advection on radiation pressure dominated accretion discs.

For bound-free and free-free absorption ( $A_{\text{R}} = 1, B_{\text{R}} = -\frac{5}{2}$ ), it can be shown that in this case the disc is stable with respect to thermal and viscous instability for all  $\beta_p$ .

It needs to be stated that these results are only based on a local stability analysis and it still needs to be shown by either time-dependent simulations or a global stability analysis when these unstable modes are operational.